UCRL - 2699
cy 2

UNIVERSITY OF CALIFORNIA

Radiation Laboratory

TWO-WEEK LOAN COPY

This is a Library Circulating Copy which may be borrowed for two weeks. For a personal retention copy, call Tech. Info. Division, Ext. 5545

BERKELEY, CALIFORNIA

DISCLAIMER

This document was prepared as an account of work sponsored by the United States Government. While this document is believed to contain correct information, neither the United States Government nor any agency thereof, nor the Regents of the University of California, nor any of their employees, makes any warranty, express or implied, or assumes any legal responsibility for the accuracy, completeness, or usefulness of any information, apparatus, product, or process disclosed, or represents that its use would not infringe privately owned rights. Reference herein to any specific commercial product, process, or service by its trade name, trademark, manufacturer, or otherwise, does not necessarily constitute or imply its endorsement, recommendation, or favoring by the United States Government or any agency thereof, or the Regents of the University of California. The views and opinions of authors expressed herein do not necessarily state or reflect those of the United States Government or any agency thereof or the Regents of the University of California.

UCRL-2699

UNCLASSIFIED

UNIVERSITY OF CALIFORNIA

Radiation Laboratory

Contract No. W-7405-eng-48

DISINTEGRATION OF OXYGEN BY 300-MEV NEUTRONS

Melvin Otis Fuller

(Thesis)

September 25, 1954

Berkeley, California

Printed for the Atomic Energy Commission

DISINTEGRATION OF OXYGEN BY 300-MEV NEUTRONS

Contents

Abstract 3

I. Introduction 4

II. Results 7

III. Discussion 35

- Star Yield as a Function of Neutron Energy 35
- Characteristics of Oxygen Stars 36
- The Low-Energy Particles 37
- The Fast Particles 38
- Nature of the Star-Formation Process 39

IV. Experimental Procedure 41

- Summary 41
- Production and Recording of Events 41
  - Neutron Beam 41
  - Cloud Chamber 41
  - Photography 42
  - Operation Cycle 42
- Measurements and Reduction of Observations 48
  - Reprojection Apparatus 48
  - Method of Measuring 48
  - Ionization Estimates and Prong Identification . . . 49
  - Acceptance Criteria 49
  - Calculations 50
  - Use of Keysort Cards 50
  - Errors in Measurements and Calculations 50

Acknowledgments 53

Appendixes 54

- I. Scatter Diagrams for Two-Prong Stars 54
- II. Representative Stars in Oxygen Gas 56
- III. Transformation From Angles α and β to Angles ϕ and θ 58

References 60

DISINTEGRATION OF OXYGEN BY 300-MEV NEUTRONS

Melvin Otis Fuller

Radiation Laboratory, Department of Physics,
University of California, Berkeley, California

September 25, 1954

ABSTRACT

The 300-Mev neutron beam of the Berkeley cyclotron was used to produce disintegrations of oxygen nuclei in an oxygen-filled cloud chamber situated in a 21,700 gauss pulsed magnetic field. Pictures of the "stars" thus formed were reprojected and measured, permitting identification of most of the ejected particles and computation of their energies and momenta. Each star consisted of one or more tracks due to heavy particles of one or two charges, plus the track of the recoil nucleus. The random selection of 602 stars show approximate percentages according to total prongs as follows: 2 prong, 42%; 3 prong, 29%; 4 prong, 12%; 5 prong, 12%; 6 prong, 4%; 7 prong, 1%; plus one 8-prong star. Energy measurements of the prongs showed 29% as having over 15 Mev, 16% over 50 Mev, and 8% over 100 Mev. Using 15 Mev as a division point for slow and fast particles, the slow particles were 37% alphas, 33% protons, and 22% deuterons, and the fast particles 66% protons, 20% deuterons, and 9% alphas. The energy spectra of the slow particles show maxima at about 2, 3 and 4 Mev for the protons, deuterons, and alphas, respectively, and have the general form characteristic of evaporation spectra. The fast particles, mostly protons, exhibit energy and angular distributions similar to those previously found for heavier elements using nuclear cascade theory. The disintegration is interpreted in terms of fast particles due to the nuclear cascade process in combination with evaporation of slow particles from the excited intermediate nucleus remaining after the cascade process.

DISINTEGRATION OF OXYGEN BY 300-MEV NEUTRONS

Melvin Otis Fuller

(Thesis)

Radiation Laboratory, Department of Physics
University of California, Berkeley, California

September 25, 1954

I. INTRODUCTION

The presence of nuclear stars has long been noted, both in cloud chamber photographs and nuclear emulsions. Both of these experimental methods employ sensitive media containing oxygen in varying amounts, and oxygen is of course present in most organic substances that might be subject to bombardment by high-energy particles. The artificial production of high-energy beams of neutrons as well as of protons (in recent years) offers opportunities for the more detailed study of reactions which these particles induce in various nuclei, at energies approaching those involved in observed stars of cosmic-ray origin.

The evaporation theory of Weisskopf[1] and more recently Le Couteur,[2] based on the Bohr[3] theory of the compound nucleus, has been used to describe the evaporation of particles from the nucleus after excitation by an energetic particle. With the advent of the high-energy accelerators, this has been recognized as describing only part of the process of high-energy interaction. The discussion of such interactions by Serber,[4] in terms of the collisions of individual nucleons within the nucleus proper, and using the concept of a mean free path in nuclear matter, led to Goldberger's development of the intranuclear cascade theory.[5] In this theory the nucleus is considered as a mixture of two nonintersecting Fermi gases of neutrons and protons. The incoming high-energy nucleon reacts with this in a series of individual nucleon-nucleon scatterings. These are computed using experimental cross sections. Application of the Pauli exclusion principle requires both colliding particles to end in states outside the occupied spheres in momentum space, thus reducing the effective cross sections. High-energy forward protons should appear in charge-exchange scatters, but a dip in the distribution at small forward angles

is predicted, as momentum states corresponding to the complementary neutrons in these cases are already filled. In general, successive collisions occur, resulting in ejection of fast protons and neutrons, after which the intermediate nucleus, with a certain excitation energy, evaporates particles until it attains a state of at least quasi stability. The Monte Carlo method is employed, with certain assumptions regarding the statistical distributions of factors affecting the collisions, to obtain predictions of angular and energy distributions of the ejected particles. The results of treating a certain number of interactions by this method are thus supposed to have the same statistical fluctuations as those which will appear for the observed results of the same number of events occurring in the laboratory.

The experiments of Hadley and York[6] using 90-Mev neutrons on carbon, copper, and lead, and of Brueckner and Powell[7] using the same on carbon, generally supported the calculations of Goldberger. In particular, however, the predicted dip in the forward direction of the angular distribution of the particles was not found by Hadley and York, and fast deuterons and tritons were identified among the ejected particles. This latter was explained by the theory of the pickup process as given by Chew and Goldberger.[8]

More recently Bernardine, Booth, and Lindenbaum[9] have made a test of the Goldberger model for 'Ag-Br' stars in emulsions using both neutrons of around 300 Mev and protons at 400 Mev. They obtained agreement between their calculations and experimental results, though neither had sufficient angular resolution to test for a narrow forward dip. The tedious computations of the Monte Carlo method have since been done by computer by McManus, Sharpe, and Gellman.[10] They obtained more extensive predictions for aluminum, "silver-bromine," and uranium for both neutrons and protons at various energies between 90 and 700 Mev. Their angular distribution curves[11] again indicate the possibility of the forward dip as originally predicted by Goldberger.

The study of oxygen stars induced by 300-Mev neutrons is thus of interest from several points of view. The element is between carbon, for which experimental results at a lower energy are available, and

aluminum, for which calculations have been made as noted above. As it is an n-alpha type nucleus, evidences of alpha-particle substructure may appear. Any characteristic or predominant features of the disintegration will aid in the identification of oxygen stars as they appear as an impurity in studies of other nuclei.

The use of the cloud chamber is uniquely suited to the problem in that all isotopes of hydrogen and helium can (within limits) be identified, the determination of particle energies is good for both high and low values, and the angular resolution afforded in conjunction with the use of neutrons as bombarding particles offers a close check on the angular distribution of the ejected particles. Using 300-Mev neutrons, this method constitutes the first opportunity for such a study of the complete disintegration of oxygen, as the mean neutron energy is more than twice the total binding energy of the oxygen nucleus.

II. RESULTS

A total of 602 stars from oxygen was measured, yielding the information given in the graphs and tables following this discussion on pages 10 through 34. The nomenclature adopted is this: the total number of prongs in a star determines its class, the particular set of identities of prongs of a star determines its type.

Table I shows the absolute and relative yields as determined for the 85 types of stars identified, arranged in classes, and ordered within class according to the numbers of protons, deuterons, etc. The totals of the various particles constituting the prongs of the stars, grouped according to class, are presented in Table II (page 14). The yields of charged particles of energies above the values of 15 Mev, 50 Mev, and 100 Mev are given for each class of star in Table III. The numbers of stars having multiplicities of such prongs are given in Table IV. For Table V, the particles of different identities were considered separately, and the numbers of each found in each of the energy groups are presented.

The distributions in energy of the slower particles are given separately for each particle identity in Figs. 1 and 2. While the division into slow and fast particles has been made at 15 Mev, values up to 40 Mev are included to show the basis on which the division was made, as noted in the discussion of the following section. Figs. 3 and 4 show various fast-particle energy distributions. Protons from the most abundant star types were used to study the relation between the energy and the forward peaking of the angular distributions of prongs. For these graphs, as shown in Fig. 5, an additional division point at 200 Mev was used to make a total of five energy groups. The over-all angular distributions of all fast particles, fast deuterons, and fast protons are shown in Figs. 6, 7, and 8. Fig. 9 shows the solid-angle distribution of the fast protons only. McManus et al.[10] have computed the expected distributions in angle and energy for cascade particles from aluminum bombarded by neutrons at energies of 160 and 400 Mev. They have furnished histograms which are reproduced in Figs. 10 and 11 for comparison with my results as shown in Figs. 3, 6, and 8.

A better picture of the over-all relationship existing between energies and angles of emission of both the fast and slow particles can be gained from a scatter diagram--each prong represented as a point on a chart with energy as ordinate and scatter angle as abscissa. Two such diagrams, as drawn for protons and deuterons from the two prong stars, are included as Appendix I.

As there is no basis for postulating azimuthal asymmetry in either the fast or slow particle distributions, the study of these made in cloud chamber experiments is for the purpose of checking experimental equipment and measuring techniques. The forward 60° cone, containing a large fraction of the tracks, was used for the plot shown in Fig. 12.

Owing to the low velocity of the compound nucleus, the evaporation spectrum for particles from heavy nuclei has generally been assumed symmetrical in the laboratory angle θ. In the present experiment, this assumption cannot be made. A definite forward peaking of the evaporated particles was found, as shown in Fig. 13a. I interpret this as due to a forward velocity of the intermediate nucleus resulting from transfer of momentum during the capture of the slower knock-on nucleons within the nucleus, before the evaporation process begins. It was found that a suitable center-of-mass velocity for an "average" intermediate nucleus could be chosen which, assuming isotropic distribution in the moving system, gave the observed forward-to-rear ratios of particles in the laboratory system. This value is approximately half that which would result from the coalescence of a 300-Mev neutron and an oxygen nucleus, with no emission of fast particles, and as such is only about one-fourth that of the median-energy evaporation protons. When this c.m. velocity is used, the observed velocities are, on the average, less than ten percent greater than the corresponding values in the c.m. system. The shape of the spectrum as observed is also somewhat broader. However, neither of the effects in this case is of sufficient magnitude to merit altering the observed spectrum outside its inherent uncertainties before applying it to the c.m. distribution. The solid-angle distributions, for this assumed center-of-mass system, have been computed for the protons, deuterons, and α-particles, and are shown in Fig. 13b.

When the summation of charges of all except the shortest prong of a star was five or less, the shortest prong was identified by charge balance. It is usually referred to as the residual nucleus. (The residual in some cases was not the shortest prong, but showed heavier ionization than a shorter alpha particle.) The measured ranges of these residual nuclei, grouped according to identity, show distributions as plotted in Figs. 14 and 15. As the range-energy relationships for particles with $Z > 2$ are not well established, the estimates of Feather[12] were used to obtain the energy values corresponding to the mean ranges; these values are shown on the curves. The corresponding momenta, in proton units, are also given.

The numbers of neutrons emitted were generally unknown. (Bernardini et al. used a number equal to that of protons, while McManus et al. estimate the average number to be more nearly twice that of the protons.) However, a certain mass number for the residual was postulated when required, and the "Q" of each reaction computed. The sums of these energies and the total energy of the prongs for each event were determined. The distribution of such sums is shown for some of the more frequently occurring reactions in Fig. 16.

The production of charged pi mesons under the conditions of this experiment has been studied by Ford,[22] and hence the eight events of that type encountered in the analysis of 600 stars are included for statistical purposes only.

TABLE I

OBSERVED YIELDS OF STARS FROM OXYGEN

BOMBARDED BY 300-MEV NEUTRONS

Line	Prong identities	No. Obs.	Fraction of n-prong stars	Fraction of total stars	No. Prongs T>15	No. Prongs T>50
	2-Prong Stars:	251	- -	0.417 ± 0.026		
1)	p, N	153	0.61 ± 0.05	0.254 ± 0.021	119	84
2)	d, N	45	.18 ± .03	.075 ± .011	23	12
3)	t, N	4	.02 ± .01	.007 ± .003	2	0
4)	a, C	7	.03 ± .01	.012 ± .004	2	1
5)	α, C	36	.14 ± .03	.060 ± .010	1	0
6)	R, R	6	.02 ± .01	.010 ± .004	-	-
	3-Prong Stars:	175	- - - -	.291 ± .022	-	-
7)	p, p, C	51	.29 ± .03	.085 ± .012	48	25
8)	p, d, C	48	.27 ± .03	.080 ± .012	44	25
9)	p, t, C	7	.04 ± .01	.012 ± .004	8	3
10)	p, a, B	4	.02 ± .01	.007 ± .003	5	2
11)	p, α, B	26	.15 ± .02	.043 ± .009	22	14
12)	p, (?), R	3	.02 ± .01	.005 ± .003	3	3
13)	p, (π), 0	1	.01 ± .01	.002 ± .002	1	1
14)	p, R, R	3	.02 ± .01	.005 ± .003	3	2
15)	d, d, C	11	.06 ± .02	.018 ± .006	9	5
16)	d, a, B	1	.01 ± .01	.002 ± .002	1	1
17)	d, α, B	8	.05 ± .01	.013 ± .004	5	1
18)	t, a, B	1	.01 ± .01	.002 ± .002	0	0
19)	a, α, Be	3	.02 ± .01	.005 ± .003	1	0
20)	α, α, Be	5	.03 ± .01	.008 ± .004	2	1
21)	α, (π), N	1	.01 ± .01	.002 ± .002	1	1
22)	α, Li, Li	2	.01 ± .01	.003 ± .002	1	1

TABLE I - (Cont.)

OBSERVED YIELDS OF STARS FROM OXYGEN

BOMBARDED BY 300-MEV NEUTRONS

Line	Prong identities	No. Obs.	Fraction of n-prong stars	Fraction of total stars	No. Prongs T >15	No. Prongs T >50
	4-Prong Stars:	74	- -	0.123 ± 0.014	-	-
23)	p, p, p, B	2	0.03 ± 0.02	0.003 ± 0.002	2	1
24)	p, p, d, B	14	.19 ± .05	.023 ± .006	21	11
25)	p, p, t, B	1	.01 ± .01	.002 ± .002	2	1
26)	p, p, α, Be	9	.12 ± .04	.015 ± .005	14	7
27)	p, p, Li, Li	3	.04 ± .02	.005 ± .003	3	2
28)	p, p, π, N	2	.03 ± .02	.003 ± .002	3	2
29)	p, d, d, B	6	.08 ± .03	.010 ± .004	11	6
30)	p, d, t, B	1	.01 ± .01	.002 ± .002	1	0
31)	p, d, α, Be	10	.14 ± .04	.017 ± .005	11	5
32)	p, d, Li, Li	1	.01 ± .01	.002 ± .002	2	1
33)	p, t, α, Be	1	.01 ± .01	.002 ± .002	1	1
34)	p, a, a, Li	1	.01 ± .01	.002 ± .002	1	1
35)	p, a, α, Li	1	.01 ± .01	.002 ± .002	0	0
36)	p, α, α, Li	9	.12 ± .04	.015 ± .005	7	3
37)	d, d, d, B	1	.01 ± .01	.002 ± .002	2	2
38)	d, d, α, Be	1	.01 ± .01	.002 ± .002	0	0
39)	d, t, t, B	1	.01 ± .01	.002 ± .002	0	0
40)	d, a, a, Li	1	.01 ± .01	.002 ± .002	1	1
41)	d, a, α, Li	1	.01 ± .01	.002 ± .002	0	0
42)	a, a, a, α	1	.01 ± .01	.002 ± .002	2	0
43)	a, α, α, α	2	.03 ± .02	.003 ± .002	1	0
44)	α, α, α, α	5	.07 ± .03	.008 ± .004	2	0

TABLE I - (Cont.)

OBSERVED YIELDS OF STARS FROM OXYGEN

BOMBARDED BY 300-MEV NEUTRONS

Line	Prong identifies	No. Obs.	Fraction of n-prong stars	Fraction of total stars	No. Prongs T >15	No. Prongs T >50
	5-Prong Stars:	70	- -	0.116 ± 0.014		
45)	p, p, p, p, Be	1	0.01 ± 0.01	0.002 ± 0.002	1	0
46)	p, p, p, a, Li	1	.01 ± .01	.002 ± .002	1	1
47)	p, p, p, α, Li	5	.07 ± .03	.008 ± .004	10	2
48)	p, p, d, t, Be	1	.01 ± .01	.002 ± .002	2	1
49)	p, p, d, a, Li	1	.01 ± .01	.002 ± .002	1	1
50)	p, p, d, α, Li	6	.09 ± .04	.010 ± .004	12	8
51)	p, p, t, a, Li	1	.01 ± .01	.002 ± .002	2	1
52)	p, p, a, α, α	2	.03 ± .02	.003 ± .002	4	4
53)	p, p, π, α, B	1	.01 ± .01	.002 ± .002	1	1
54)	p, p, α, α, α	13	.19 ± .05	.022 ± .006	12	6
55)	p, d, d, d, Be	1	.01 ± .01	.002 ± .002	3	0
56)	p, d, d, α, Li	3	.04 ± .02	.005 ± .003	5	3
57)	p, d, t, α, Li	1	.01 ± .01	.002 ± .002	1	1
58)	p, d, a, α, α	7	.10 ± .04	.012 ± .004	11	4
59)	p, d, α, α, α	12	.17 ± .05	.020 ± .005	14	8
60)	p, t, a, α, α	1	.01 ± .01	.002 ± .002	2	0
61)	p, t, α, α, α	1	.01 ± .01	.002 ± .002	0	0
62)	p, t, π, α, B	1	.01 ± .01	.002 ± .002	1	0
63)	p, π, α, α, Be	1	.01 ± .01	.002 ± .002	0	0
64)	d, d, d, d, Be	1	.01 ± .01	.002 ± .002	0	0
65)	d, d, d, α, Li	1	.01 ± .01	.002 ± .002	1	0
66)	d, d, a, a, α	1	.01 ± .01	.002 ± .002	4	3
67)	d, d, a, α, α	2	.03 ± .02	.003 ± .002	2	1
68)	d, d, α, α, α	3	.04 ± .03	.005 ± .003	2	0
69)	d, t, a, a, α	1	.01 ± .01	.002 ± .002	3	1
70)	d, t, α, α, α	1	.01 ± .01	.002 ± .002	1	1

TABLE I - (Cont.)

OBSERVED YIELDS OF STARS FROM OXYGEN

BOMBARDED BY 300-MEV NEUTRONS

Line	Prong identifies	No. Obs.	Fraction of n -prong stars	Fraction of total stars	No. Prongs T > 15	No. Prongs T > 50
	6-Prong Stars:	26	- -	0.043 ± 0.008	-	
71)	p, p, p, p, α, α	1	0.04 ± 0.04	0.002 ± .002	3	0
72)	p, p, p, d, α, α	6	.23 ± .09	.010 ± .004	11	6
73)	p, p, p, t, a, α	1	.04 ± .04	.002 ± .002	2	1
74)	p, p, p, t, α, α	1	.04 ± .04	.002 ± .002	3	0
75)	p, p, d, d, a, α	2	.08 ± .05	.003 ± .002	3	2
76)	p, p, d, d, α, α	8	.31 ± .11	.013 ± .004	14	8
77)	p, d, d, d, a, a,	1	.04 ± .04	.002 ± .002	0	0
78)	p, d, d, d, α, α	5	.19 ± .09	.008 ± .004	10	5
79)	p, d, π^-, α, Li	1	.04 ± .04	.002 ± .002	1	1
	7-Prong Stars:	5	- -	.008 ± .004	-	-
80)	p, p, p, p, p, d, α	1	0.20 ± 0.20	.002 ± .002	1	1
81)	p, p, p, p, d, t, a	1	.20 ± .20	.002 ± .002	2	1
82)	p, p, p, d, d, t, α	1	.20 ± .20	.002 ± .002	4	1
83)	p, p, d, d, d, t, a	1	.20 ± .20	.002 ± .002	4	2
84)	p, p, d, d, d, t, α	1	.20 ± .20	.002 ± .002	3	1
	8-Prong Stars:					
85)	p, p, p, p, p, p, p, d	1	- - - -	.002 ± .002	3	1

Key: p - proton, d - deuteron, t - triton, a - He^3, α - He^4

The last two columns give the numbers of prongs of energies greater than 15 and 50 Mev respectively found in stars of each type. The uncertainties shown on the fractional yields are standard deviations due to counting statistics alone.

Table II

Particle Yields from Oxygen Stars

Class of Star	Particles Identified						Ratio
	p	d	t	a	α	π^-	H/He
2	153	45	4	7	36	0	4.65
3	194	79	8	9	50	2	4.76
4	94	46	5	11	68	2	1.84
				*(1)	(26)		(2.79)
5	100	58	8	18	136	3	1.07
				*(10)	(102)		(3.86)
6	55	45	2	5	46	1	2.00
				*(4)	(40)		----
7	16	10	4	2	3	0	6.00
				*(0)	(1)		----
8	7	1	0	0	0	0	----
Totals	619	284	31	52	339	8	2.38
% yield	46.5	21.3	2.3	3.9	25.4	0.6	
Totals minus *()	619	284	31	37	170	8	4.48
% yield	53.9	24.7	2.7	3.2	14.8	0.7	

* Particles interpreted as being due to low-energy splitting of nucleus remaining after ejection of fast prongs.

Table III

Yields of Fast Particles from Oxygen

Class of Stars	No. of Stars	Total Prongs	Total Prongs with T>15 Mev	Average Number per Star	Fraction of Total Prongs	Total Prongs with T>50 Mev	Average Number per Star	Fraction of Total Prongs	Total Prongs with T>100 Mev	Average Number per Star	Fraction of Total Prongs
2	251	502	147	0.59	0.29	97	0.39	0.19	63	0.25	0.13
3	175	525	156	0.89	0.30	85	0.49	.16	44	.25	.08
4	74	296	88	1.19	0.30	44	0.59	.15	25	.34	.08
5	70	350	95	1.36	0.27	55	0.79	.16	14	.20	.04
6	26	156	48	1.84	0.31	23	0.88	.15	8	.31	.05
7	5	35	14	2.80	0.40	6	1.20	.17	2	.40	.06
8	1	8	3	3.0		1	1.0		0		
TOTALS	602	1872	547	0.91	0.29	303	0.50	0.16	156	0.26	0.08

The numbers at higher energies are included in those at lower energies.

Note that the fractional yields, using total prongs, are nearly constant for all classes of stars within each energy group. Also, of the fraction having T>15, just about half have T>50, and again half of this second number have T>100.

Table IV

Multiplicity of Fast Prongs in Oxygen Stars

Class of Stars	No. in Class	Numbers of stars in class having n prongs with energies greater than 15 Mev				50 Mev			100 Mev	
		n= 1	2	3	4	1	2	3	1	2
2	251	147 (.59)	-	-	-	97 (.39)	-	-	63 (.25)	-
3	175	107 (.61)	24 (.14)	-	-	77 (.44)	4 (.02)	-	44 (.25)	-
4	74	32 (.43)	19 (.26)	5 (.07)	-	36 (.49)	4 (.05)	0	23 (.31)	1 (.01)
5	70	26 (.37)	22 (.31)	5 (.07)	3 (.04)	34 (.49)	5 (.07)	1 (.01)	14 (.20)	0
6	26	7 (.27)	9 (.35)	6 (.23)	1 (.04)	11 (.42)	6 (.23)	0	4 (.15)	2 (.08)
7	5	1	1	1	2	4	1	0	2	0
8	1	0	0	1	0	1	0	0	0	0
Totals	602	320	75	18	6	260	20	1	150	3
Fraction of total stars.		.531	.125	.030	.010	.432	.033	.002	.249	.005

Showing the numbers of stars of each class having one, two, or more prongs of energy at least that given at the top of the group. Numbers in higher-energy groups are included in totals of lower energy.

Numbers in parantheses show fraction of stars in that class.

Table V

Particle Yields per Energy Group--by Identity

Particle / No. obs.	T<15		15<T<50		50<T<100		100<T<200		200<T		Total Fast (T>15)		*Hadley & York 20<T<90
p / (616)	253 / (0.41)	0.33	129 / (0.21)	0.53	95 / (0.15)	0.65	97 / (0.16)	0.85	42 / (0.07)	0.95	363 / (0.59)	0.66	0.60
d / (279)	170 / (0.61)	0.22	55 / (0.20)	0.23	38 / (0.14)	0.26	14 / (0.05)	0.12	2 / (0.01)	0.05	109 / (0.39)	0.20	0.36
t / (30)	19 / (0.63)	0.03	9 / (0.30)	0.04	2 / (0.07)	0.01	0		0		11 / (0.37)	0.02	0.04
a / (52)	34 / (0.65)	0.05	10 / (0.19)	0.04	6 / (0.12)	0.04	2 / (0.04)	0.02	0		18 / (0.35)	0.03	-
α / (329)	283 / (0.86)	0.37	39 / (0.12)	0.16	6 / (0.02)	0.04	1 / (0.01)	0.01	0		46 / (0.14)	0.09	-

Particles identified and for which energy was established, in five energy groups. The numbers in parentheses beneath yield numbers show fraction of that particle yield; the fractions to right of yield numbers show fraction of that energy group.

*Fractional yields of protons, deuterons, and tritons as obtained by Hadley and York for 90-Mev neutrons on carbon. (Reference 6.)

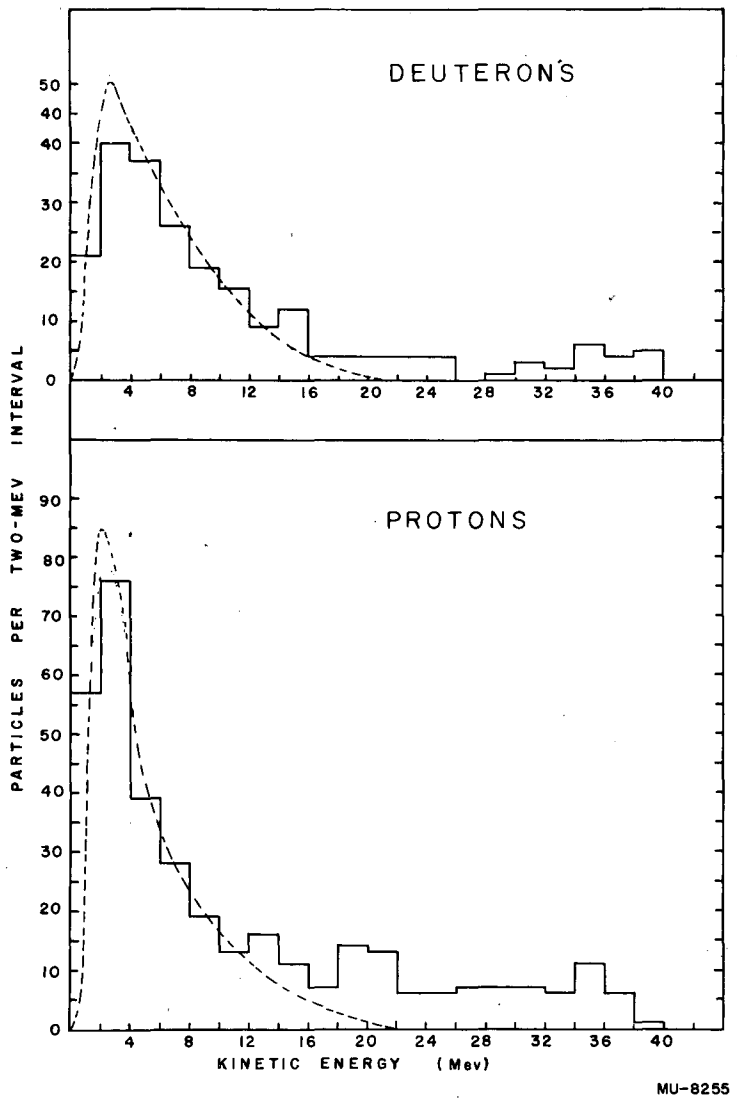

Fig. 1 Protons and deuterons of energies below 40 Mev produced by 300-Mev neutrons on oxygen.

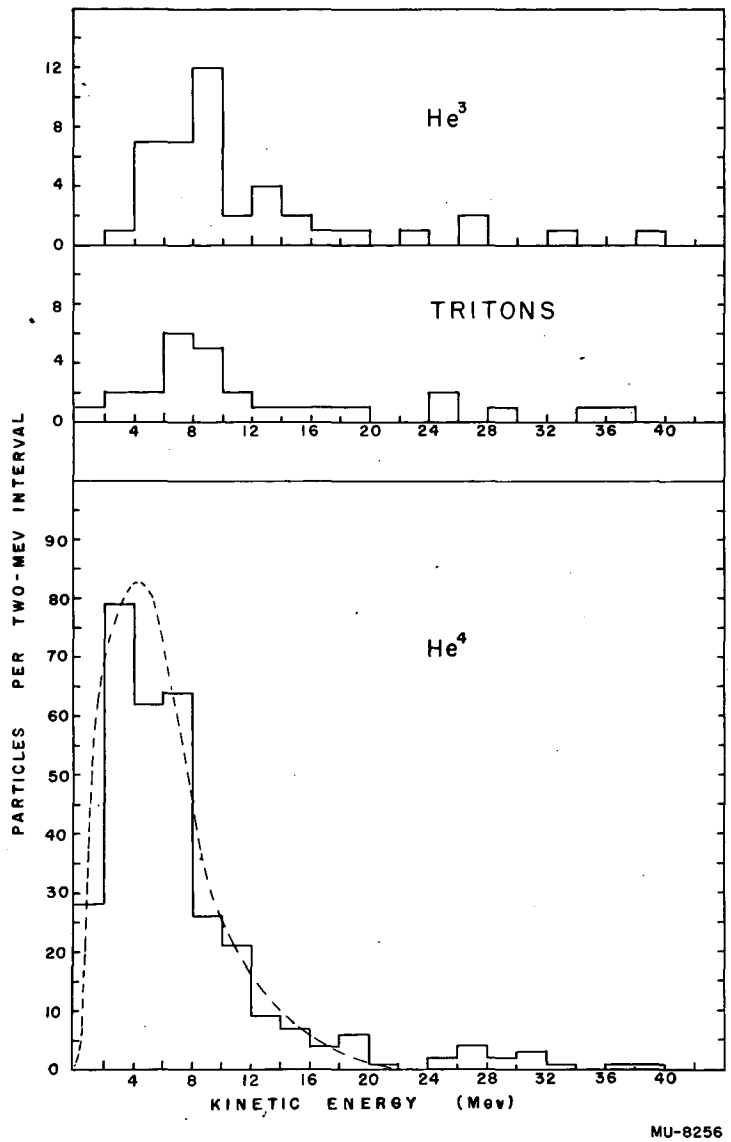

Fig. 2 He^3, tritons, and alpha-particles of energies below 40 Mev produced by 300-Mev neutrons on oxygen.

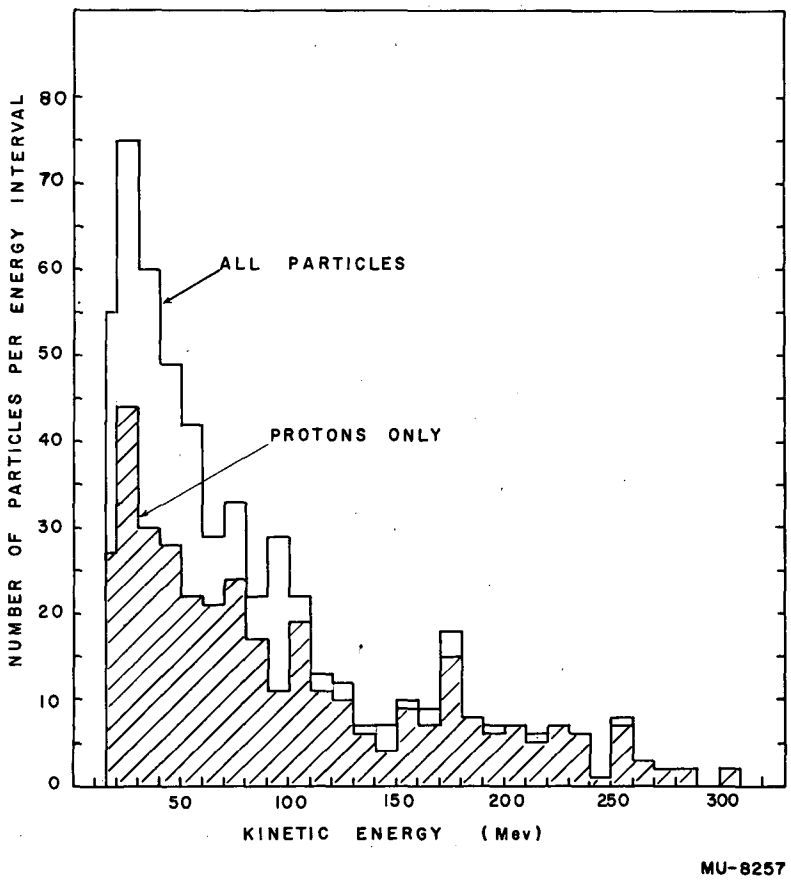

Fig. 3 Energy distribution of fast particles from oxygen.

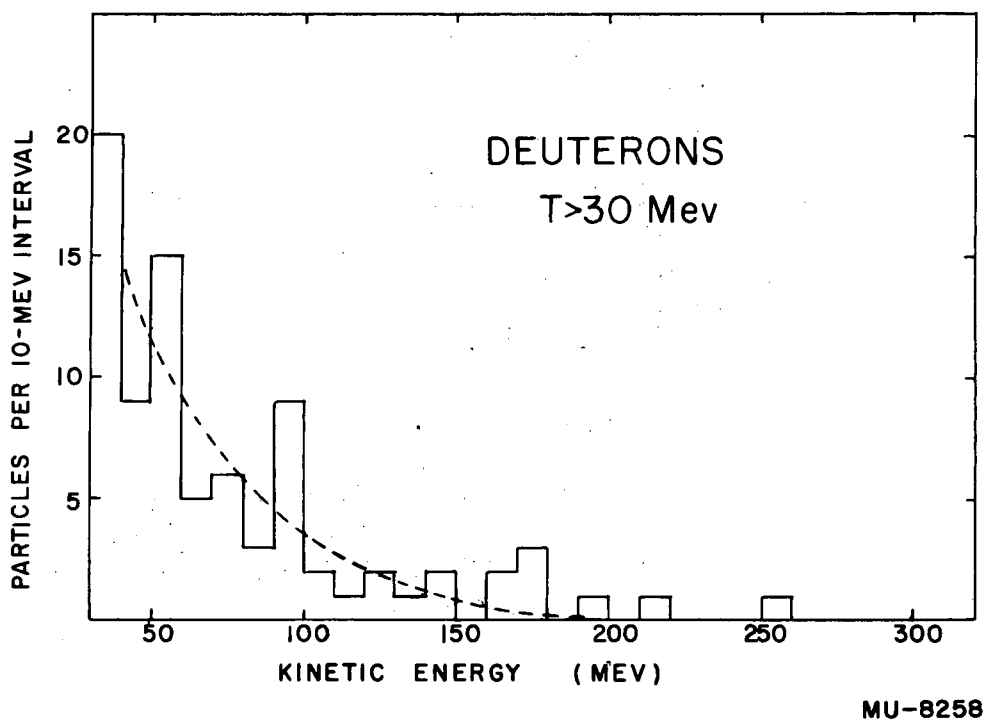

Fig. 4 High-energy deuterons from oxygen. The dotted curve is from Bransden,[16] using arbitrary normalization.

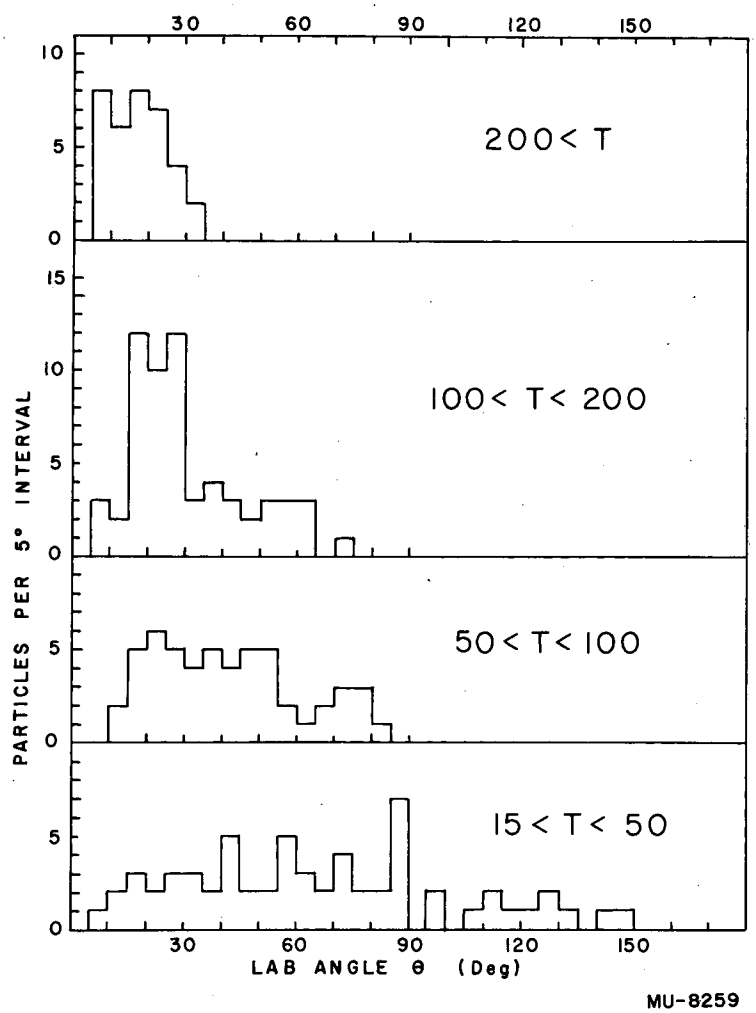

Fig. 5 Angular distributions of protons of various energies.

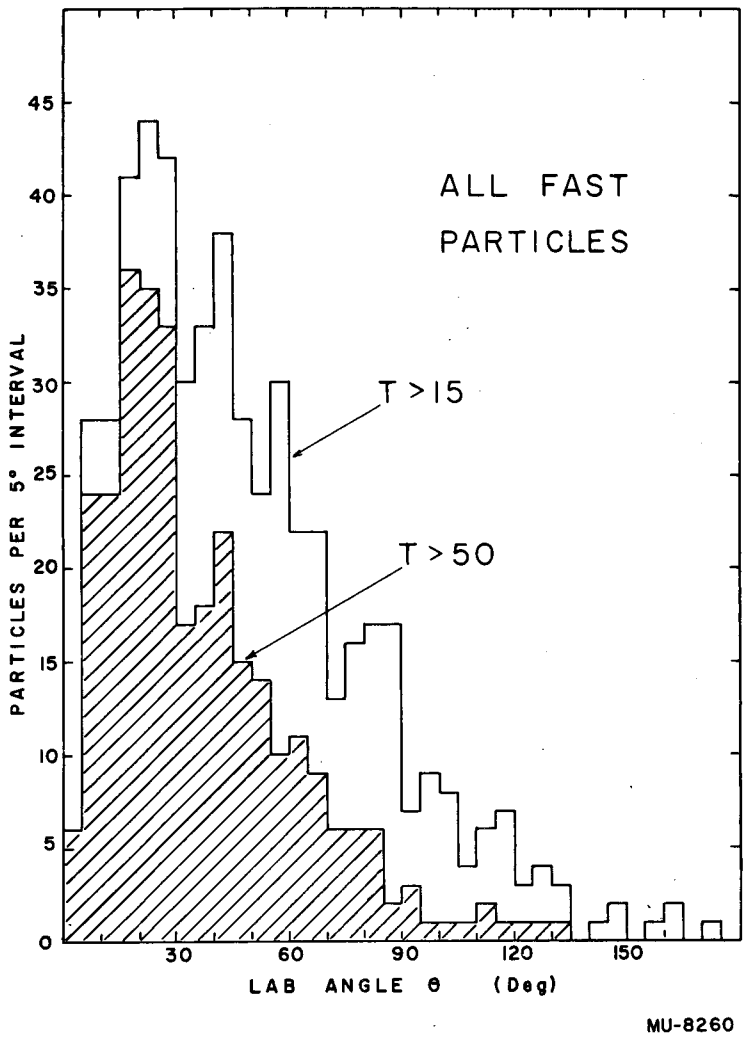

Fig. 6 Angular distribution of all fast particles.

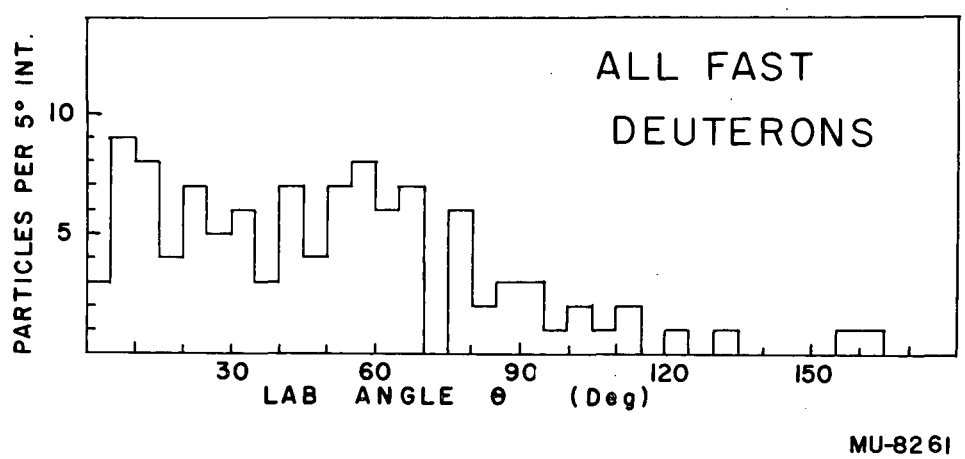

Fig. 7 Angular distribution of fast deuterons.

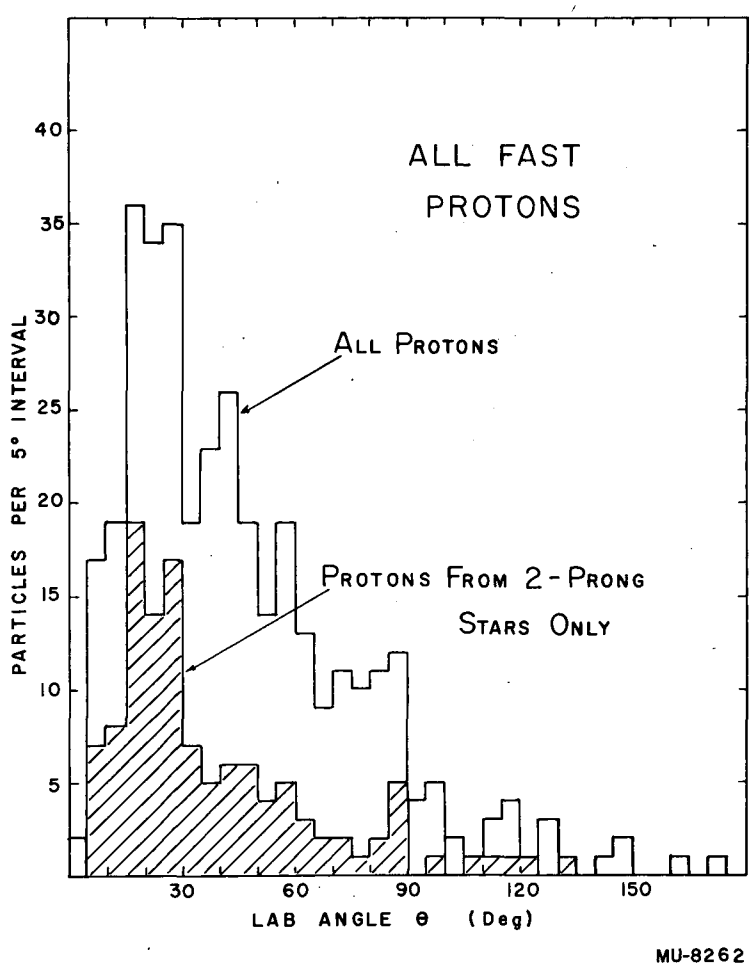

Fig. 8 Angular distribution of fast protons from oxygen.

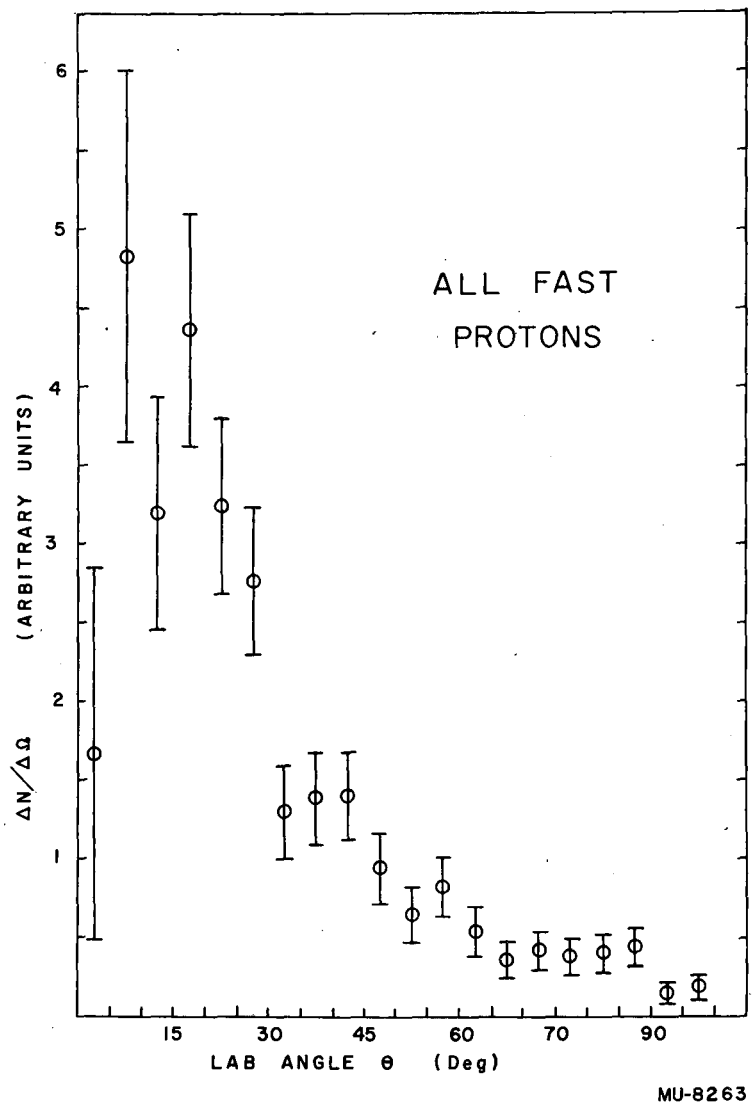

Fig. 9 Solid-angle distribution of fast protons from oxygen. Errors shown are those due to counting statistics alone.

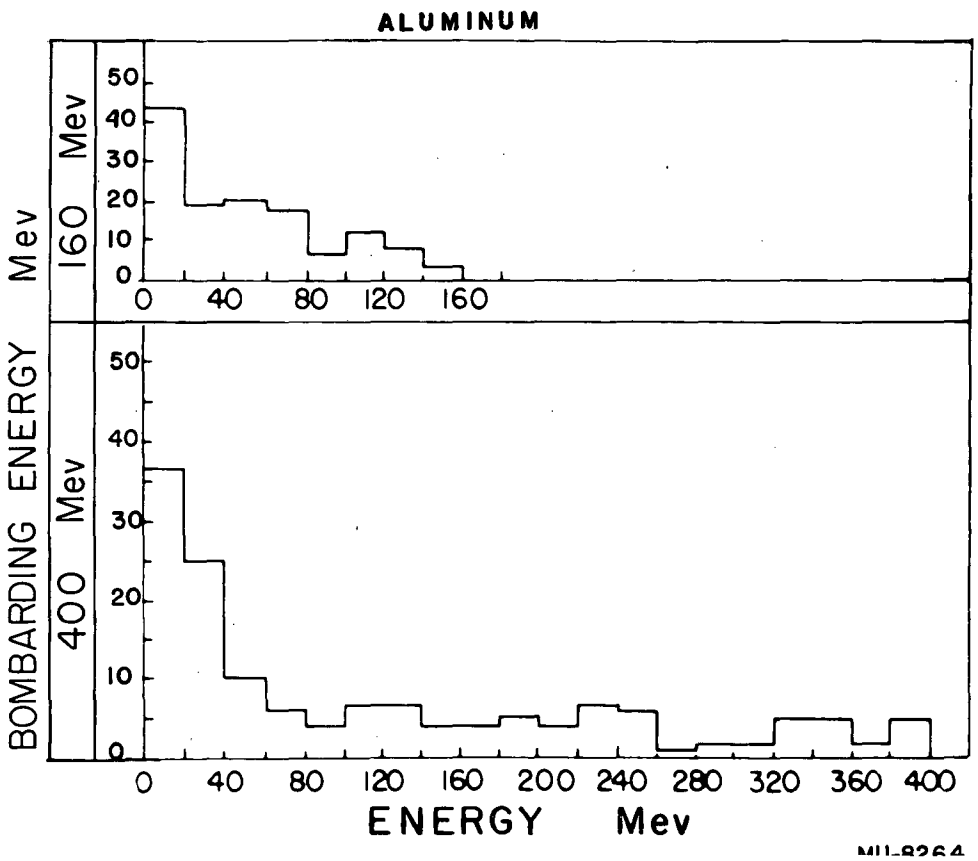

Fig. 10 Energy distribution of fast particles (protons and neutrons) computated for aluminum under conditions shown. Taken from reference 11. This may be compared with Fig. 3 above.

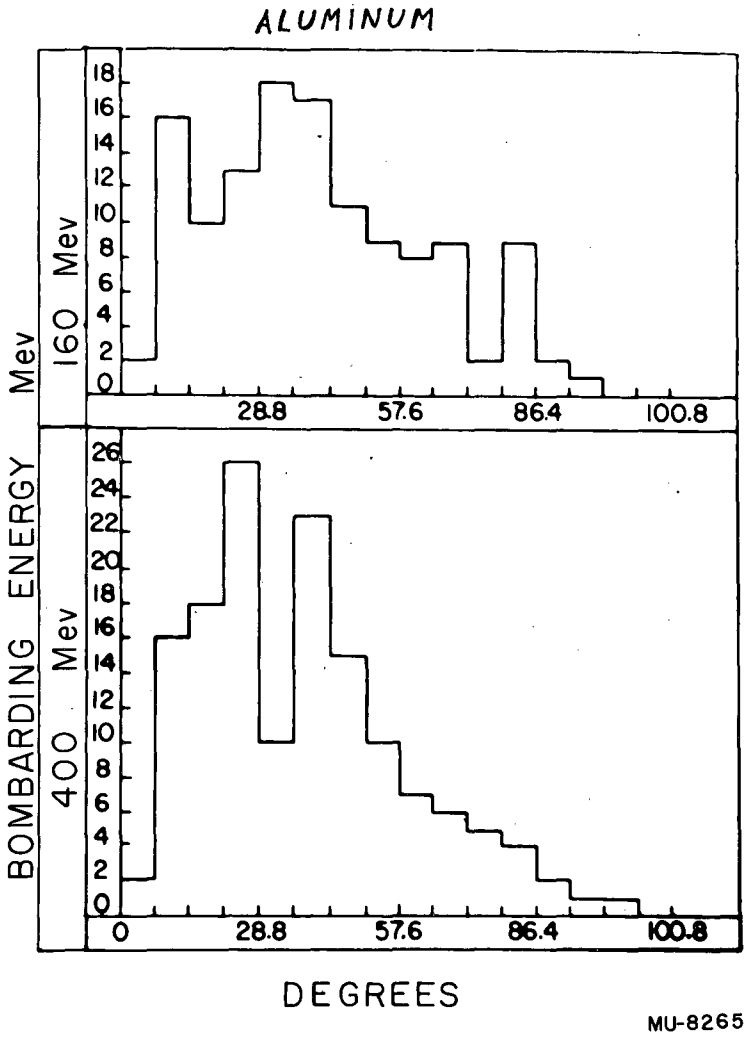

Fig. 11 Angular distribution of fast particles for aluminum. Taken from reference 11. This may be compared with Figs. 6 and 8 above.

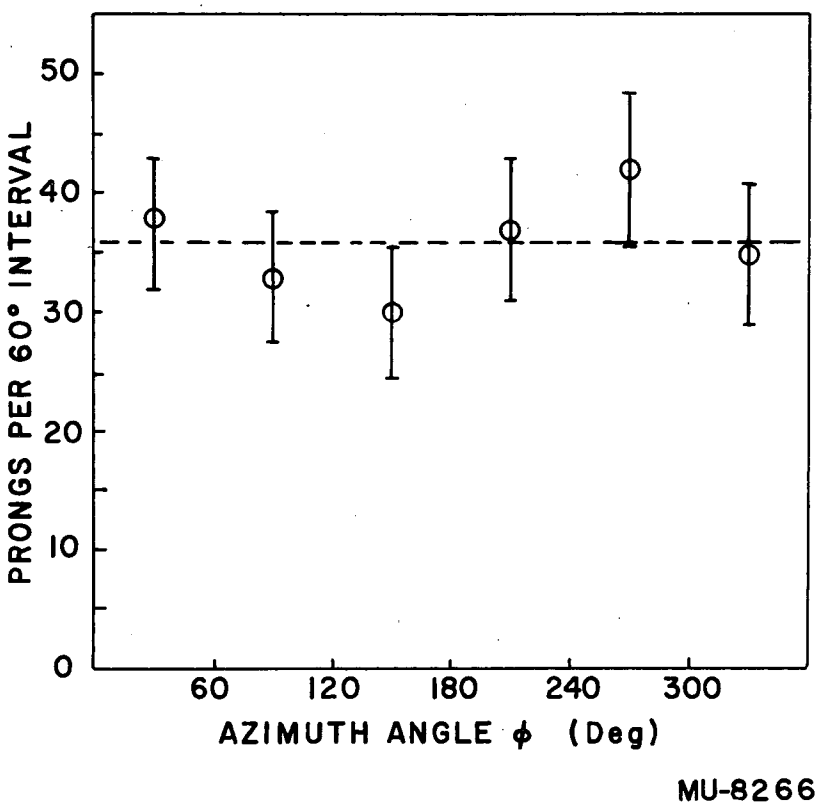

Fig. 12 Azimuthal distribution of prongs. The particles considered in this analysis were all protons and deuterons from lines 1, 2, 7, and 8 of Table I having beam angle θ less than 60°.

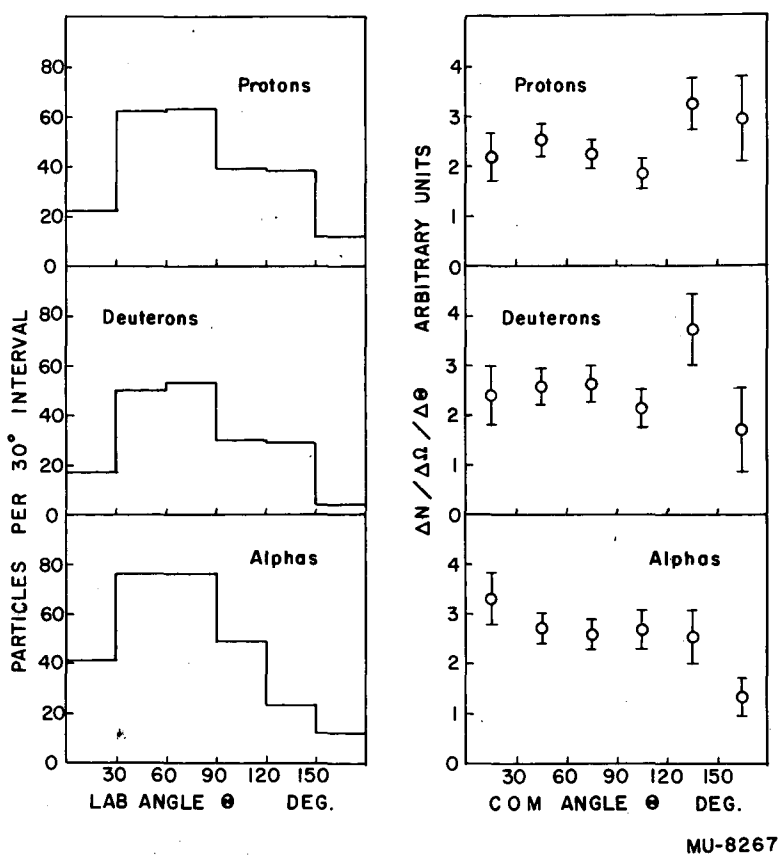

Fig. 13a Fig. 13b

Angular distributions of the evaporation particles. The observed distributions for protons, deuterons, and alphas are shown in (a). The computed solid-angle distributions for an assumed center-of-mass system (discussed under "Results") are shown in (b).

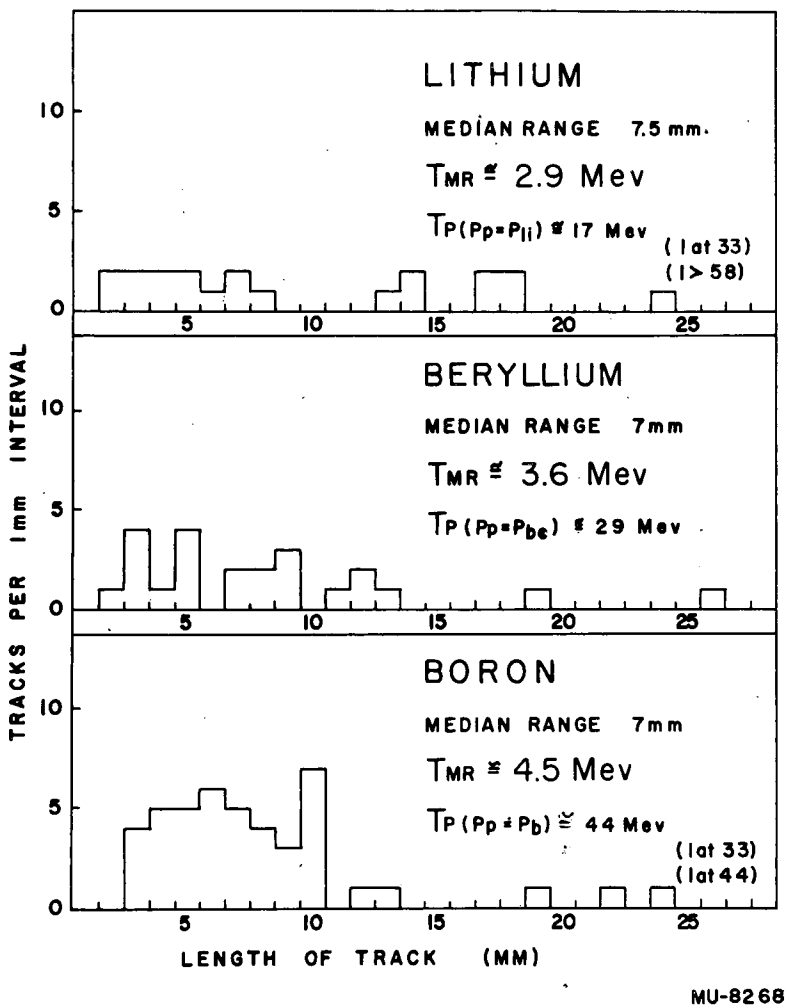

Fig. 14 Ranges of residual nuclei: lithium, beryllium, and boron. The median ranges were used with the estimates of Feather[12] to compute kinetic energies. The lower figures give the energies of protons having momenta equal to those of the residuals.

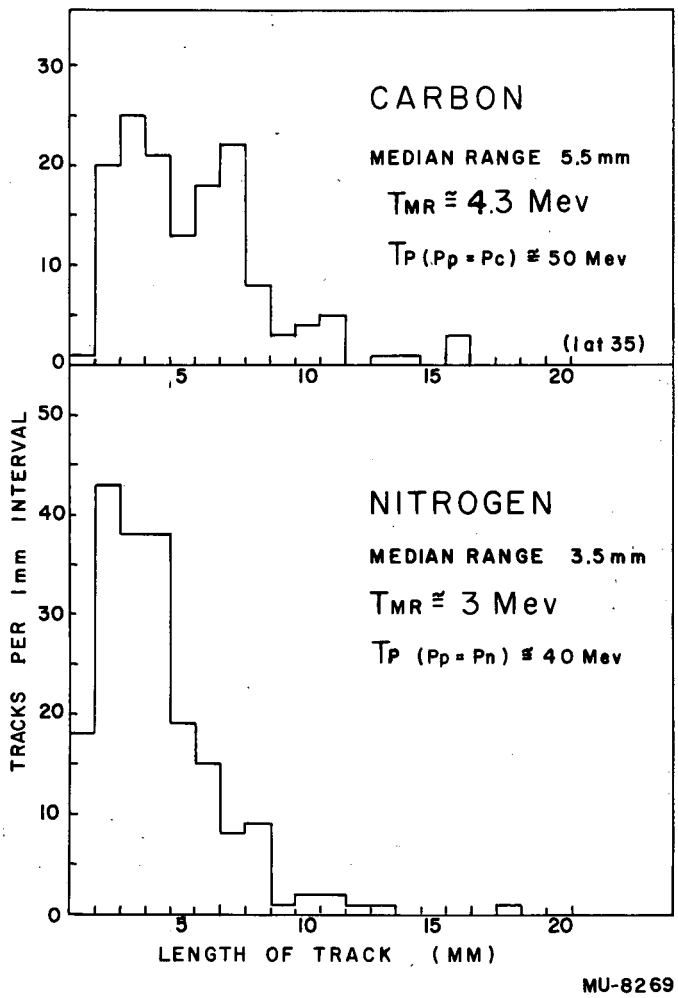

Fig. 15 Ranges of residual nuclei: carbon and nitrogen. (See previous picture for explanation of figures.)

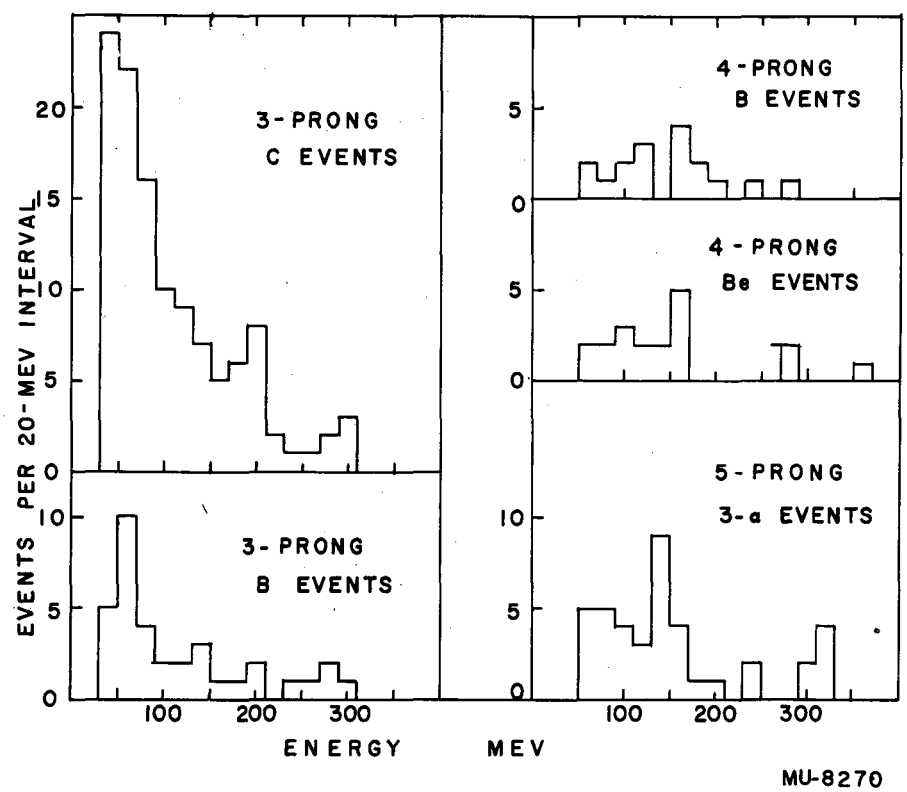

Fig. 16 Distribution of the sums of prong energies and reaction thresholds for the more abundant types of stars in oxygen.

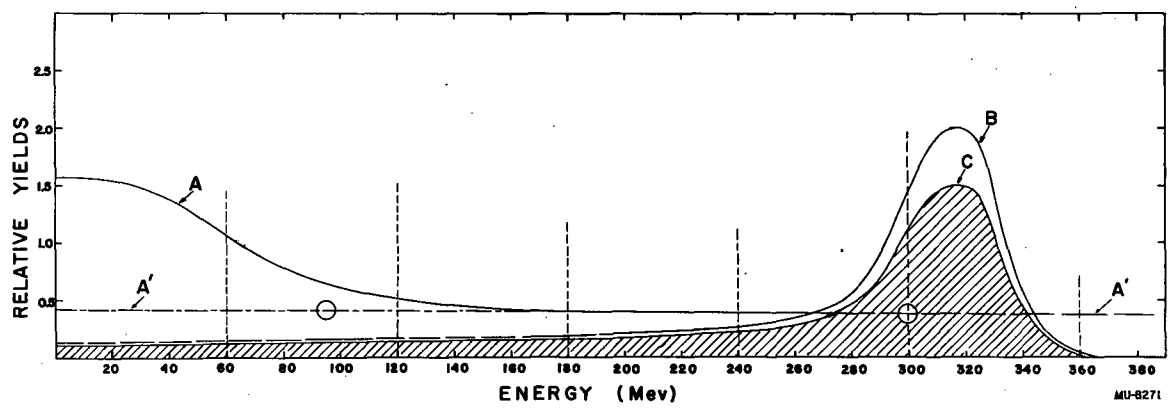

Fig. 17 Relative yield of oxygen stars as a function of energy. Shaded area gives net result. (See text following for explanation of curves and method).

III. DISCUSSION

Star Yield as a Function of Neutron Energy

The measurements made on the oxygen stars allow computations of only the necessary minimum energy of the incident neutron for each star. As the numbers and energies of the emitted neutrons (including the incident neutron which has transferred part of its energy to target nucleons) are unknown and largely indeterminable, the actual energy of the incident neutron responsible for a given star cannot generally be found. If the over-all problem is considered, however, an estimate of the magnitude of the star yield as a function of neutron energy may be obtained. This was done by making use of the neutron-energy spectrum of the beam, the total cross section for neutrons on oxygen as a function of energy, and the relative values of the inelastic part of the total cross section as a function of energy. The graphical combination of these is shown in Fig. 17. The neutron-energy spectrum, curve B, is from Ball;[13] this was extended to lower energies on the basis of preliminary results from similar targets[14] indicating that the low-energy tail is essentially flat. The total cross-section curve is from reference 15, and was extended linearly to higher energies. This curve was multiplied at the points 95 and 300 Mev by the fraction of the total due to inelastic reactions, taken from Ball,[13] to give the two circled points. The line A'-A' through these points was multiplied point by point by the curve B to obtain the final curve C. This was taken as the final yield curve. This was divided into 60-Mev sections, as shown, and the relative yields were determined by planimeter measurements to be as follows:

Neutron Energy Range	Percent of Yield
$300 < T$	47
$240 < T < 300$	23
$180 < T < 240$	10
$120 < T < 180$	7
$60 < T < 120$	7
$T < 60$	6

The uncertainties of the values thus obtained are necessarily quite large, due chiefly to those of the neutron spectrum, as may be seen in Fig. 20. A certain number of the events making up the inelastic cross section do not produce stars (recoils and multiple neutron emission). The above procedure assumes that this number forms a constant fraction of the inelastic cross section for all energies.

Characteristics of Oxygen Stars

The 602 stars due to neutron disintegration of oxygen studied in this experiment presented a wide variety in appearance and apparent energy, ranging from 251 two-prong events to a single eight-prong star. The more outstanding characteristics of these may be seen by examination of the tables and graphs above, and are summarized below.

Two- and three-prong stars together constitute more than 70% of the total observed yield. Each of these has a residual prong averaging about 0.5 centimeter in length -- an α-particle of this length would have an energy of about 1.5 Mev. The longest prong in more than 50% of these is a proton of over 15 Mev. In more than 40% of the stars of two or three prongs the most energetic prong shows more than 50 Mev. Deuterons occur at both high and low energies in about 20% of these stars. Alpha particles are somewhat less frequent and almost always of low energy.

The lesser numbers of stars with higher numbers of tracks may show energetic prongs of various identities, even at large angles to the beam direction. Protons are still the most abundant of the fast prongs, but α-particles predominate at low energies. It seems remarkable that the fraction of prongs occuring with energies greater than 15 Mev remains constant for all classes of stars, and that the fraction is again constant for prongs with energies above 50 Mev. Any multiplicities of fast prongs in single stars occur very infrequently, only about 8% of all stars having two prongs of more than 15 Mev each, and only 3% having three such prongs. The incidence of doubly-charged particles is particularly high in the five-prong stars; only four out of seventy have no such prong, and over 60% have three and consequently no residual. The occurrence of high numbers of α-particles as compared to those of deuterons is discussed further in the next section.

The Low-Energy Particles

The outstanding features of the yields of particles of low energies resulting from the disintegration of oxygen at high energies are (1) the relatively high numbers of α-particles and deuterons in comparison with protons, and (2) the short lengths of the 'tails' appearing on the energy-distribution curves for the different particles.

The splitting of a low-Z nucleus such as carbon or beryllium into alpha particles at low excitation energies is by now a well-recognized phenomenon. The high rate of incidence of the alphas as observed here is possibly due to a similar splitting of such nuclei in the roles of intermediate nuclei in the disintegration of oxygen, any requisite energy in this case being obtained from the residual excitation energy remaining after the ejection of the fast particles. The frequent appearance of the α-particles in pairs or triplets lends weight to the argument. The deuterons at these low energies may also be at least partially explained on the basis, again, that it is energetically cheaper to evaporate such particles than the two nucleons separately.

The energy distributions of the slow particles, shown in Figs. 1 and 2, show peaks at from 2 to 5 Mev, thereafter falling off rapidly up to around 12 Mev. The appearance of these curves lends support to the assumption that they represent the evaporation spectra for the various particles from the excited intermediate nucleus. Above the 12-Mev value, the distributions are essentially flat, and tend to show the characteristics of the cascade process curves previously cited. The computed curve of McManus et al.,[11] Fig. 10, shows peaks at the lowest energy intervals, but the peaks are less than those evident on the present low-energy particle curves. The curves drawn on the figures represent a best guess as to the division of the observed particles into evaporation and cascade groups. The value of 15 Mev, chosen as distinguishing between the slow and fast particles, is thus an attempt to fix a basis for assigning approximately the correct numbers of particles to each of the two processes. It is not intended to represent either the upper limit of the evaporation spectra or the lower limit of the cascade spectra of the particles.

The upper ends of the evaporation spectra, as drawn, indicate that very few of these particles have energies greater than 20 Mev. If an average (counting residual nuclei and neutrons) of about three evaporation particles per star is used, the excitation energy involved is estimated to be of the order of 20 to 25 Mev. This may be compared with the computed values of McManus et al.[11] for aluminum: averages of 25 and 29 Mev, corresponding to incident neutron energies of 160 and 400 Mev.

The solid-angle distributions of the protons, deuterons, and α-particles, as shown in Fig. 13b, are interpreted as indicating symmetry in the assumed center-of-mass system. Although such a system is purely a mathematical fiction, the results indicate that the evaporation particles are emitted isotropically.

The Fast Particles

The high incidence of protons among the fast particles from oxygen, particularly above 100 Mev, is of course an expected result. Several high-energy deuterons are observed in this region of energies at small angles to the beam. They can be assigned to a primary pickup process involving the incident neutron and a proton of the target nucleus. At lower energies the numbers of fast deuterons and tritons are comparable with previous experimental results using neutron beams of that energy range. This indicates that we may attribute the observed particles to pickup reactions between the more energetic of the knock-on particles from the incident neutron and other target nucleons. This idea is further substantiated by the observation that these pickup particles are found at fairly large angles to the beam direction. (Note the scatter diagrams for deuterons and tritons from two-prong stars in Appendix I.) The theory of such a secondary pickup process for deuteron formation has been given by Bransden.[16] The observed energy distribution of deuterons, Fig. 4, is consistent with his prediction of the energy distribution for the secondary process. Considering the energy distributions at particular angles, the number of particles herein observed does not allow any extensive analysis. Within statistics, however, the results are consistent with those obtained by Hess[17] for deuterons from lithium, carbon, and aluminum.

The He^3 particles, with energies and angles corresponding to those of the tritons, must be ascribed to a similar process. The small numbers of both kinds of mass-three particles observed, and the difficulty in distinguishing between them when the tracks do not end in the chamber (this is discussed in a later section) precludes the drawing of conclusions as to their relative importance in the fast-particle process.

The forward peaking of the angular distributions with energy, in particular that shown for the proton distributions, is consistent with Goldberger's prediction and with the results of previous experimental work at lower energies. The apparent dip in the forward direction, as seen in Figs. 8 and 9, probably does not exist. The uncertainty in the small number of particles observed for $\theta < 5^{\circ}$ does not allow a definite answer, but if the dip does exist it must be much narrower and probably not as deep as predicted. The over-all angular distributions, both for protons alone and for all fast particles taken together, compare favorably with the computed histograms (for aluminum) of McManus et al. A similar agreement is observed for the corresponding energy distributions of the fast particles. The present results are thus interpreted as indicating that the cascade process occurs in oxygen as the mechanism responsible for the ejection of the fast particles. As indicated in the preceeding section, the lower energy limit for the particles from this process is not clear.

Nature of the Star-Formation Process

The observed distributions in angle and energy of the particles resulting from the bombardment of oxygen by high-energy neutrons indicate the action of at least two mechanisms for their production. Assuming only two, one is a process supplying particles of energies ranging from near that of the incident neutron down 15 Mev or less, with the particles peaking strongly with energy in the forward direction. The second process clearly involves the excitation of an intermediate nucleus, with subsequent evaporation of sufficient particles to insure at least quasi stability of the residual nucleus.

The nuclear cascade theory of Goldberger,[5] as developed from Serber's model,[4] provides a likely mechanism for the first process.

If this can be applied to oxygen, and the agreement of the present work with the computations of McManus et al.[11] indicates that it can be, any modification necessary is probably about as follows. The mean free path of the incident neutrons in nuclear matter is greater than the radius of the oxygen nucleus (values are about 5×10^{-13} and 3.5×10^{-13} cm). Thus the most probable interaction involves only one of the target nucleons directly, and results in the preponderance of two- and three-prong stars. Those stars in which only a single proton is ejected cannot be considered as simple n-p scattering, as previously explained, as the Pauli principle modifies the allowed distributions. Some momentum and energy in all cases transferred to the residual nucleus, as is evident in the recoil track. In those cases wherein only a small part of the incident-neutron energy is transferred to a nucleon within the nucleus, or the larger part of its energy to another neutron, the visible evidence of the interaction consists of only a low-energy knock-on proton or evaporated particle and the residual recoil. An increasing incidence of fast particles is observed in successively fewer cases, through action of the intranuclear cascade. These occur at higher angles to the beam direction on the average, as is to be expected with the more thorough 'mixing' involved. The concomitant higher excitation energies of the residual nuclei result in the larger yields of evaporation particles accompanying the greater numbers of fast particles. The velocity of the intermediate nucleus resulting in the forward peaking of these evaporation particles is easily accounted for by the capture in the intermediate nucleus of the slower cascade particles prior to the evaporation process.

The two-part interaction postulated thus seems capable of explaining the features of the stars and their individual prongs as observed. In particular, the cascade process, with the addition of pickup reactions, is indicated as being responsible for all particles observed with energies above those of the particles due to a comparatively low-temperature evaporation process.

IV. EXPERIMENTAL PROCEDURE

The experimental procedure is presented in two parts: (1) the production and recording of events, and (2) measurement and reduction of observations.

Summary

A beam of 300-Mev neutrons was used to produce stars in oxygen gas in a Wilson cloud chamber operated in a strong magnetic field. Photographs of the events were recorded on film. Through stereoscopic reprojection of the pictures in space, measurements of track curvatures, angles, and position were made. These, together with ionization estimates or range measurements, provided a basis for identifying the star prongs and assigning values of energy and momentum. The pertinent data for each star were then entered on an especially printed Keysort data card, facilitating the computation of momentum components and allowing rapid sorting of the data to obtain the information as presented under "results".

Production and Recording of Events

The general arrangement of the experimental setup and a section of the cloud chamber assembly are shown in Figs. 18 and 19 on pages 43 and 44 following.

Neutron Beam. A beam of neutrons of nominal energy 300 Mev was produced by bombarding a 0.5-inch lithium deuteride target with a pulsed beam of 340-Mev protons. The energy spectrum of the beam has been investigated by Ball,[13] and his results are shown in Fig. 20. This beam emerges from a hole in the cyclotron shielding, and was further collimated for this experiment by a copper collimator three feet long passing a beam 2.75 inches wide and 0.75 inch high, just before entering the chamber. It then traversed the center of the chamber horizontally, entering through a 3-mil copper foil window 5 inches long by 1 inch high, and leaving through a similar window in the far wall to reduce back-scattering.

Cloud Chamber. The 22-inch-diameter cloud chamber developed by Powell[13] and used in this experiment has a plate-glass top through which the pictures are taken. On this are drawn accurately positioned fiducial marks for aligning the chamber in the neutron beam and for aligning and focusing

the pictures in the reprojection apparatus, as described subsequently. The bottom of the chamber, which moves vertically under control of the pantograph arms beneath it to effect the expansion, was covered with gelatin impregnated with black dye. This formed an excellent background for the photography of the stars and also furnished the water vapor necessary to track formation. Two GE FT422 flash tubes are mounted, approximately as shown, with suitable cylindrical lenses to light the chamber through the cylindrical lucite side walls. The beam of light thus produced gives nearly uniform illumination over the central 2-1/2 inches of the 3-1/2-inch height of the chamber in the expanded position. A clearing field is provided.

The magnetic circuit surrounding the chamber produces a known field of nominal value 21,700 gauss when energized by a 150-horsepower minesweeper generator. This is pulsed to deliver the required 400 amperes current, which remains constant over a period of about 0.15 seconds. The magnet is temperature-controlled, and the chamber may be kept at an essentially constant temperature by a circulating water system. For this run, the chamber was filled with oxygen gas to a pressure of 86 cm Hg in the expanded position. Of this pressure, about 1.8 cm was due to water vapor.

Photography. Stereoscopic pairs of photographs were taken by an especially constructed camera mounted on a lighttight crown 27 inches above the top glass of the chamber. The lenses are a matched pair of Leitz Summitars, and were used at f/6.3. The film used is Eastman Linagraph Ortho, in strips 1.8 inch wide by 100 feet long. A third lens (not shown in the figure) views a magnet-current meter and records the current through the magnet with each set of two pictures. Exposure was obtained by connecting each of the flash tubes momentarily across a 256-microfarad capacitor bank charged by a suitable 1700-volt circuit.

Operation Cycle. The cycle of operations used for the chamber is controlled by synchronization with the cyclotron pulses. The sequence of events is as follows: the magnet current is turned on, the clearing field is turned off, the chamber is expanded with the current reaching maximum just before the diaphragm hits bottom, the beam passes through the chamber just afterward, and the lights are flashed about 0.03 second after beam passage.

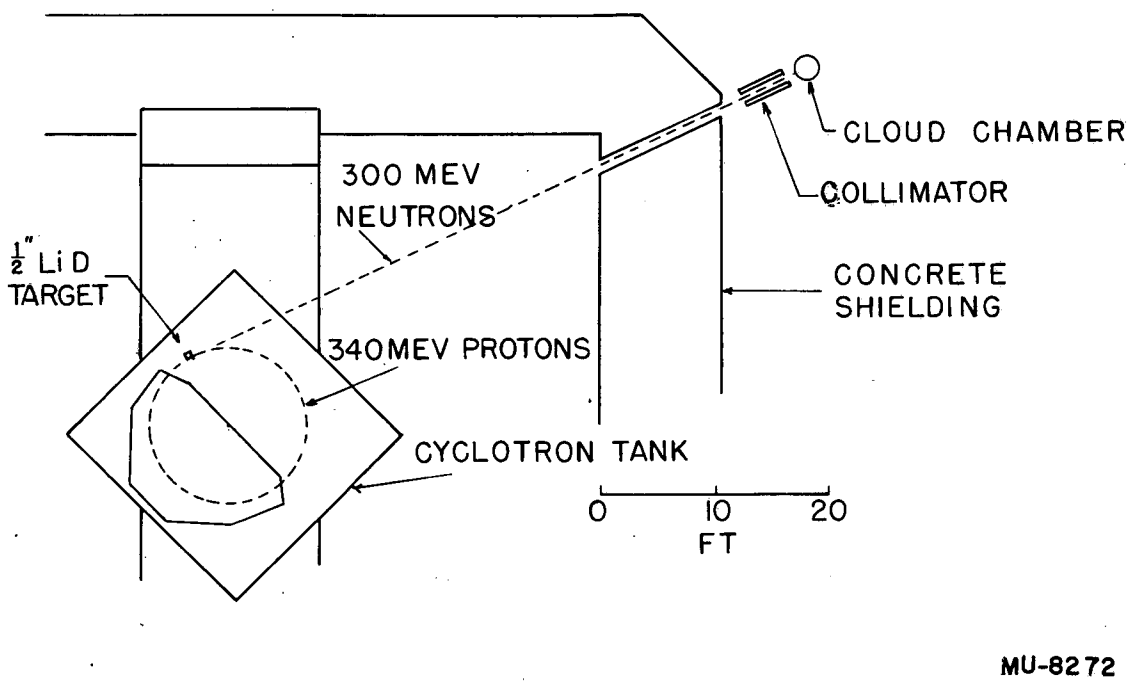

Fig. 18 Cyclotron, collimator, and cloud-chamber arrangement.

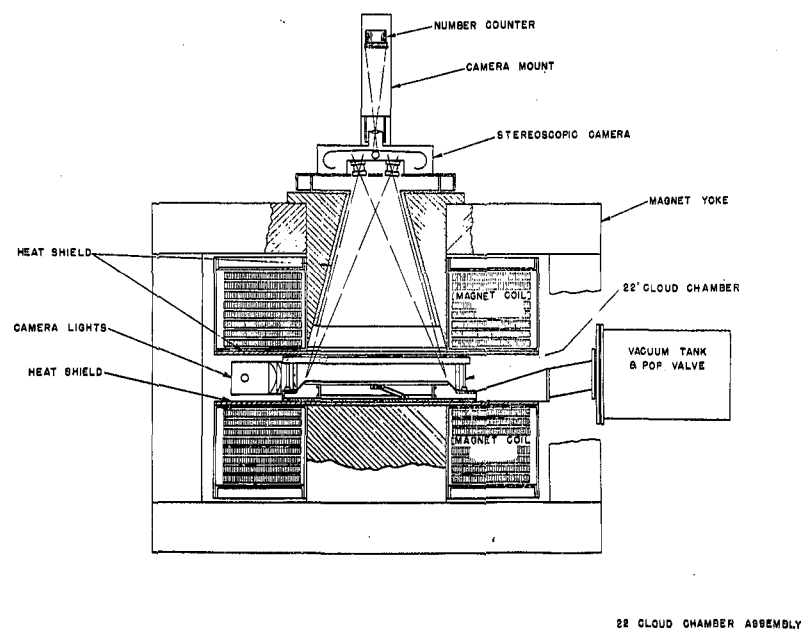

Fig. 19 Schematic cross section of cloud chamber, magnet, and camera assembly.

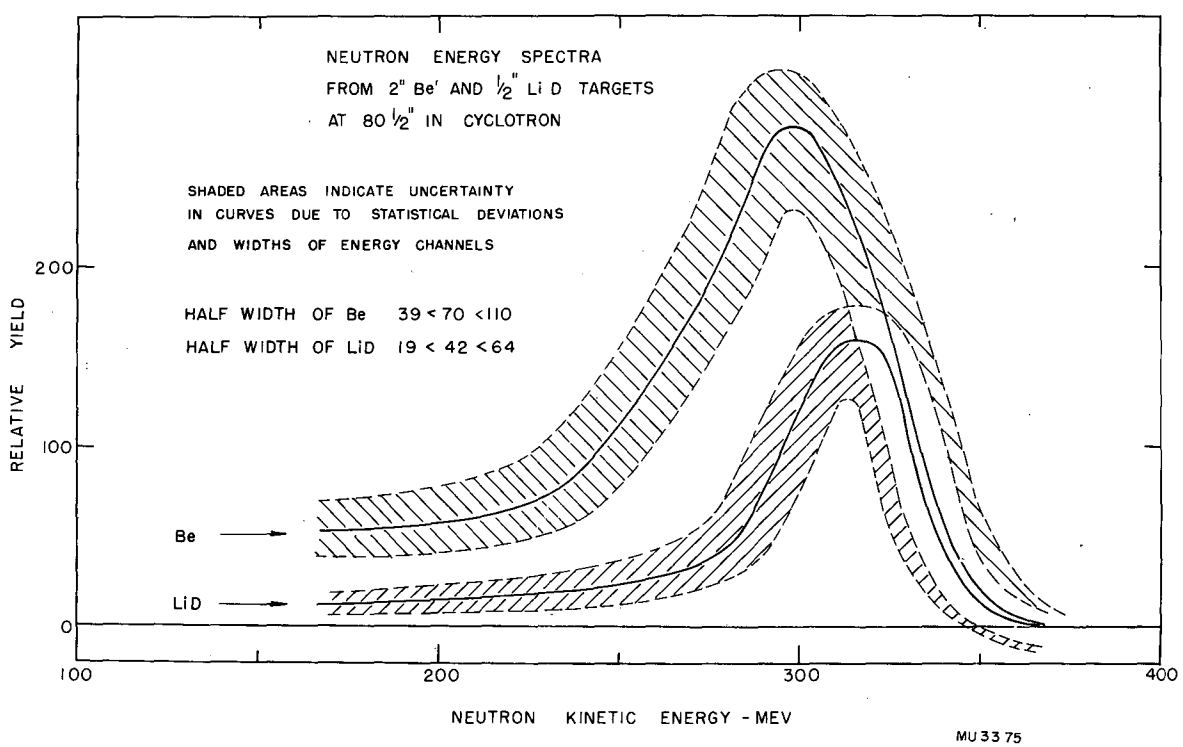

Fig. 20 Neutron energy spectrum as determined by Ball.[13] The lower curve applies to this experiment.

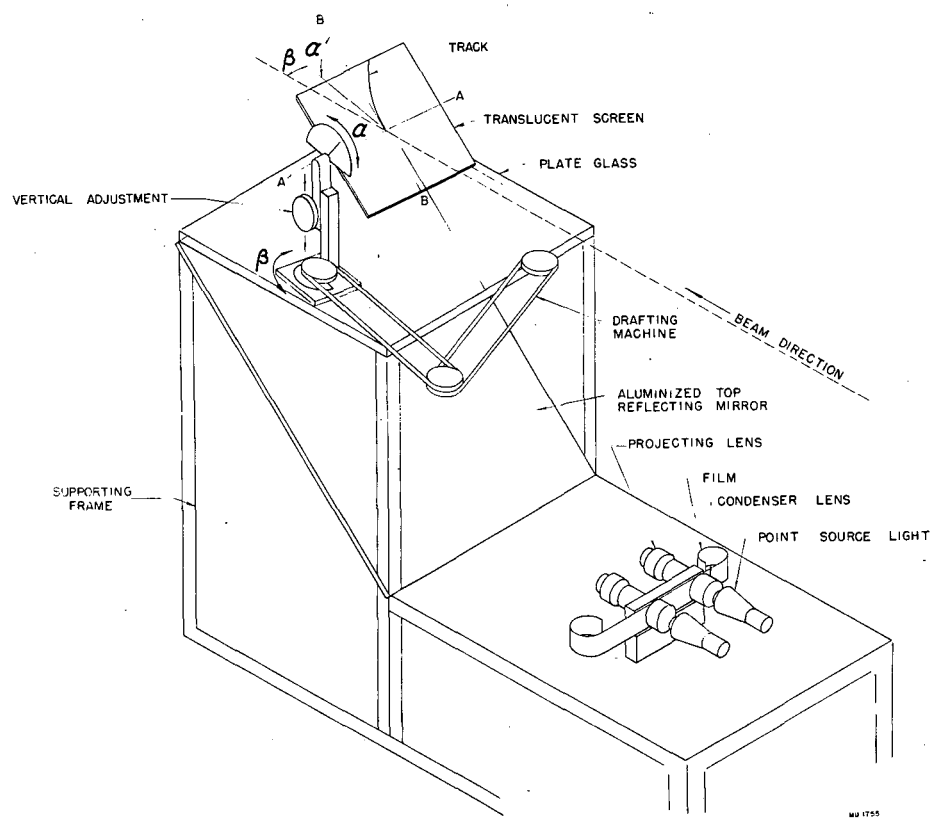

Fig. 21 Reprojection apparatus similar to that used. The explanation in the accompanying text may be followed by reference to this diagram.

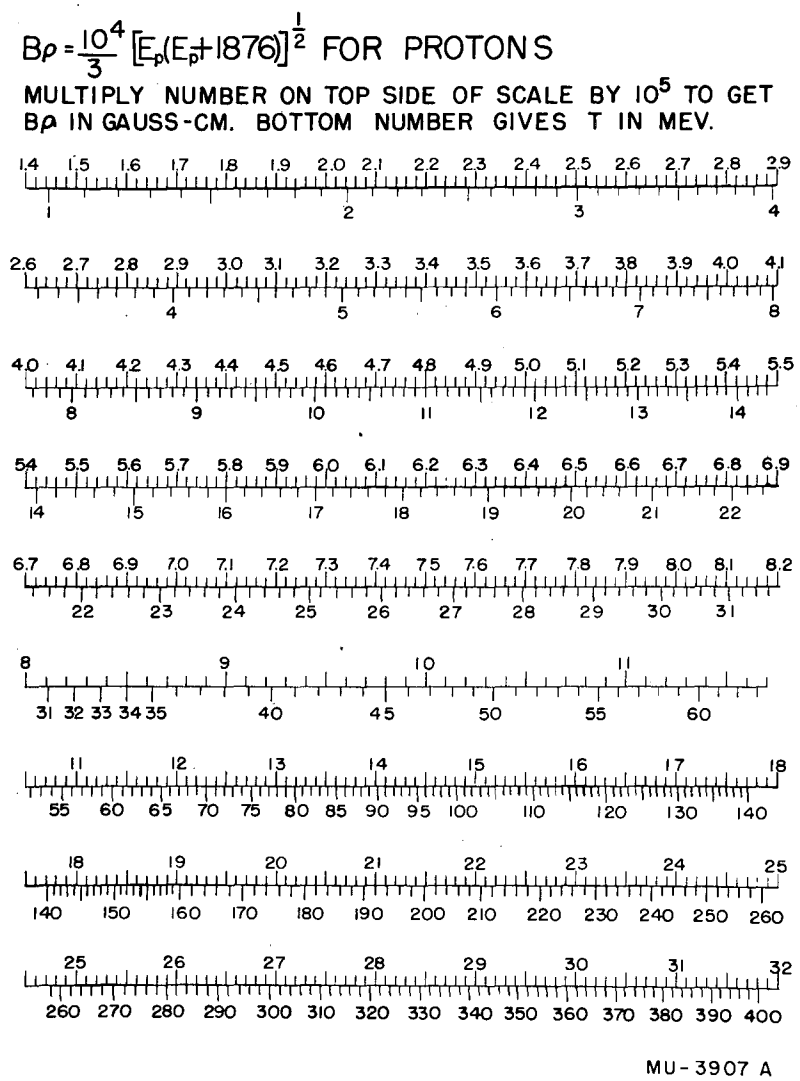

Fig. 22 $B\rho$ - E_p relation.

Measurements and Reduction of Observations

Reprojection Apparatus. The apparatus as described in reference 19 and shown in Fig. 21 differs slightly from that actually used in this experiment, but both models are operated in the same manner to obtain the same results, and the description below is in terms of the machine shown.

The camera lenses are used to reproject the images from the film into the space above the plate-glass table, where they may be caught on the translucent screen. With this screen properly centered and horizontal, and its axis B-B along the established beam-direction line and at the proper distance from the projector head, the aforementioned fiducial marks provide images allowing the proper focusing and juxtaposition of the pictures for accurate stereoscopic image formation.

Method of Measuring. The method of making measurements is as follows. After focusing as described above, one raises the screen of the projector and translates it horizontally, positioning the center of the screen at the origin of the star to be read. The table is then rotated in β (see Fig. 21) until line B-B is approximately along the first track, and then in α to obtain juxtaposition of the two track images along as much of the track as possible. By final adjustment of both rotations, one makes the line B-B tangent to the track at the origin of the star, with the star still at the center of the screen. The dip angle α and beam angle β of the tangent (and track) are now read from their respective dials, $0 \leqslant \alpha \leqslant \pm 90^{\circ}$ from the horizontal and $0 \leqslant \beta \leqslant 360^{\circ}$ from the forward beam direction in a horizontal plane. While the setting in α is retained the table is translated, and rotated in β to keep B-B tangent, so as to obtain as long a portion of the track as possible for the radius-of-curvature measurement. The measurement is made by matching to the image one of a series of accurately ruled curvature templates. This gives the slant radius of curvature, ρ'. If the track ends in the lighted portion of the chamber, a flexible ruler is used to obtain the total range of the particle. When the curvature measurement is taken, the height and radial displacement of the center of the section of track used are found by reference to the proper scales. (These are not shown on the picture.)

Ionization Estimates and Identification of Prongs. A starting scale of ionizations was provided by the presence of several tracks per picture of varying curvature (and hence of varying ionization) due to protons knocked out of the forward window by the neutron beam. A table of relative ionizations[20] for particles p, d, t, He^3, and He^4, and range-energy curves for the gas used (made by applying the proper factors to published curves for NTP air), are the standard tools for this procedure. It was found by the author that a Bausch and Lomb Spectrum-Measuring Magnifier (magnification 6.5x, scale graduations 0.1 mm) gave good measurements of the widths of tracks in the range of relative ionizations from about 10 to 100. The squares of these were roughly proportional to relative ionization density for known tracks.

Protons and deuterons have ionizations of approximate ratio 1:3 for the same curvature, and as protons are the most abundant of the particles, these two could almost always be distinguished even at low ranges. The biggest uncertainties were in distinguishing between deuterons, tritons, and He^3, particularly the latter two, for which the ionizations are in approximate ratio 3:4 for most of the fast-particle curvatures found. In general, the average of about six stars per picture provided tracks with enough different values so that a scale could be established that led to the fairly certain identification of all tracks. This was particularly true in those stars with the higher numbers of prongs, where charge balance could be used. As apparent track-density changes vary slowly when above two or three hundred, it was impossible to make any identifications of residual nuclei by that means. In the few cases where residuals were longer than 1.5 cm, they had much heavier ionizations than known α-particles of similar range in the same star or picture. A further aid in the procedure was the use of characteristic track endings, that is, tracings of tracks of known identity ending in the chamber and lying approximately in the horizontal plane. These were checked against computed curves for such particles in the gas and found to agree quite closely.

Acceptance Criteria. The horizontal projection of the neutron collimator opening through the chamber, together with two planes perpendicular to the axis of the beam passing through the end fiducial marks (12 inches apart) on the top glass, defined a rectangular parallelopiped in which the

stars must have originated to be counted and read. In any picture, all stars within that volume were used. The very low number of stars found outside this volume shows that the assumption of a parallel beam is justified. It parts of a picture were faulty, the whole picture was discarded, thus not affecting the ratios of star classes (i.e., numbers of prongs).

Calculations. The measured curvatures were multiplied by cos θ and then by the corrected value of the field to obtain the values $B\rho$. These were then entered in the $B\rho$ -versus-Energy chart, Fig. 22, to obtain the energy of each prong. For tracks for which the range was known, the range-energy curves provided the range and the $B\rho$-$E\rho$ chart then was used to obtain the momentum (in $B\rho$ units). The beam angle θ and azimuth angle ϕ were obtained by means of the formulae derived in Appendix III and the accompanying nomograph.

Use of Keysort Cards. The values of energy and momentum, the angles θ and ϕ, and identities for all prongs of the same star were then entered on an especially printed Keysort data card, a card being used for each of the 602 stars analyzed. After the values were punched into the sorting holes, the cards were easily divided into groups for computation of momentum according to octant, and thus according to the signs of the different components. Computation was by slide rule, using the usual transformation equations from spherical-polar to Cartesian coordinates. All sorting of stars and prongs into various groupings was then done by means of the cards, providing a self-checking system. The cards were carefully checked against the original data sheets to insure one-to-one correspondence.

Errors in Measurements and Calculations. The chief errors involved are due to inaccuracies in the measuring devices and to the fact that no stars were rejected because one or more tracks were at extreme angles. The latter problem is discussed separately at the end of this section.

1. Radius of curvature. The error in this measurement is that found in matching the ruled templates to the curves, which in many experiments using this procedure has amounted to 0.1 mm in the sagitta irrespective of the curvature or track length. The momentum of a particle has, on the average, an uncertainty of about ± 5 percent, and thus the energy has an uncertainty of about ± 10 percent. The effect of

turbulence in the chamber, through the examination of "no field" pictures, was found to be negligible compared to this.

2. Dip and beam angles. The total error in these due to the reprojection apparatus and procedures used has been investigated by Wilson M. Powell and his collaborators.[19] They give the figures $\pm 1.5^{\circ}$ for $0^{\circ} < \alpha < 50^{\circ}$ and $\pm 1^{\circ}$ for β.

3. Magnetic field. The total variation of the magnetic field throughout the chamber volume is about 6 percent. However, a map is available, accurate to 0.5%, which allows corrections to the assumed value. These were applied, using values for the midpoints of the tracks. As the field varies slowly and nearly linearly over the region used, this gave quite accurately the required value. The errors in energy values due to the variations in the field were thus much smaller than those introduced by the curvature measurements.

4. Acceptance of steep tracks. In order to obtain as good statistics as possible on numbers and identities of prongs, particularly for the stars with higher numbers of prongs, it was not deemed advisable to reject stars on the basis of steep tracks. In the angular distribution determined for all prongs of energy greater than 15 Mev, more than one-third of all tracks, and all of those in the forward peak, had θ-values less than 30°, and hence also had α-values less than the same amount. Of the stars in the region between the 30° forward and backward cones (in θ), only one-half would have had α-values greater than 30°. Further, if we extend the θ-values to 60°, only 36 percent of the total number of tracks is affected and of these prongs, only about one-fourth, or 9 percent of the total prongs, would have had α-values greater than 60°. The inaccuracies of tracks in the regions of $\alpha > 60^{\circ}$ are thus judged to have small effect upon the angular and energy distributions determined in this experiment.

5. Stars missed, misread, or discarded. The pictures were scanned in a stereoviewer both before and after reading, and later by an independent observer. It is fairly certain that not more than one or two, if any, two-prong stars consisting of a very steep prong and a very short residual nucleus were missed. Three two-prong stars were added by the second scanning, two additional very short prongs on larger stars,

and one long "thin" track out of a four-prong star. The discarded stars consisted of three single prongs with no residuals, two stars showing only two tracks (which were, in both stars, identified as one proton and one deuteron), and one 6-prong high-energy star for which five singly-charged prongs and one doubly-charged prong were identified. The first five of these were adjudged due to helium-three recoils and two disintegrations, and the last identified as nitrogen. They thus do not appear among the oxygen stars in the results.

ACKNOWLEDGMENTS

I wish to express my sincere appreciation to Professor Wilson Powell for suggesting the problem and for many valuable suggestions during the course of the experiment. Dr. T. C. Merkle provided help and encouragement during the earlier part of my experimental work. The cooperation and willing assistance of the several members, past and present, of the cloud chamber group is gratefully acknowledged, especially that of Mr. Howard White in suggesting and helping plan the use of the Keysort cards, and that of Mr. Peter Murphy in the sorting and tabulation.

APPENDIX I

Scatter Diagrams for Two-Prong Stars

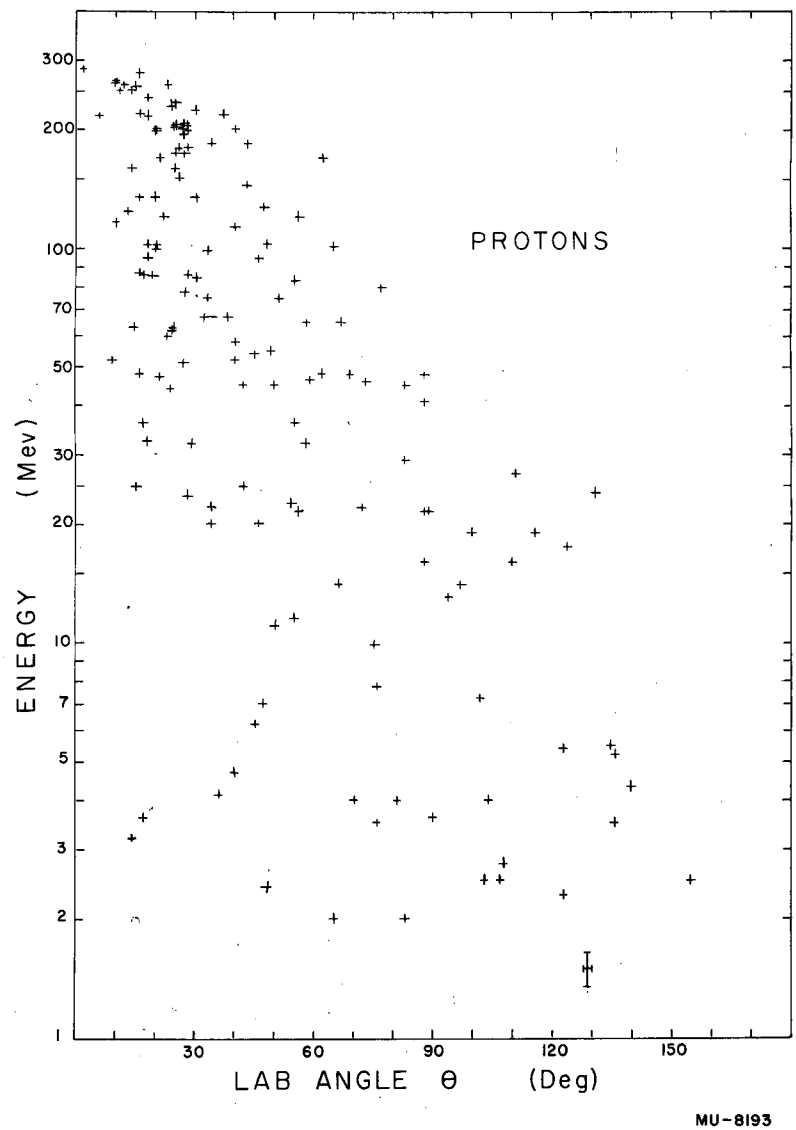

Protons from oxygen

Distribution in angle and energy of the single protons knocked out of oxygen (line 1 of Table I) by 300-Mev neutrons. The symbol for the lowest-energy proton shows the uncertainty (for any point) in angle θ of $\pm 1^{\circ}$ and that in energy of $\pm$ 10%, and is to scale at any position on the diagram.

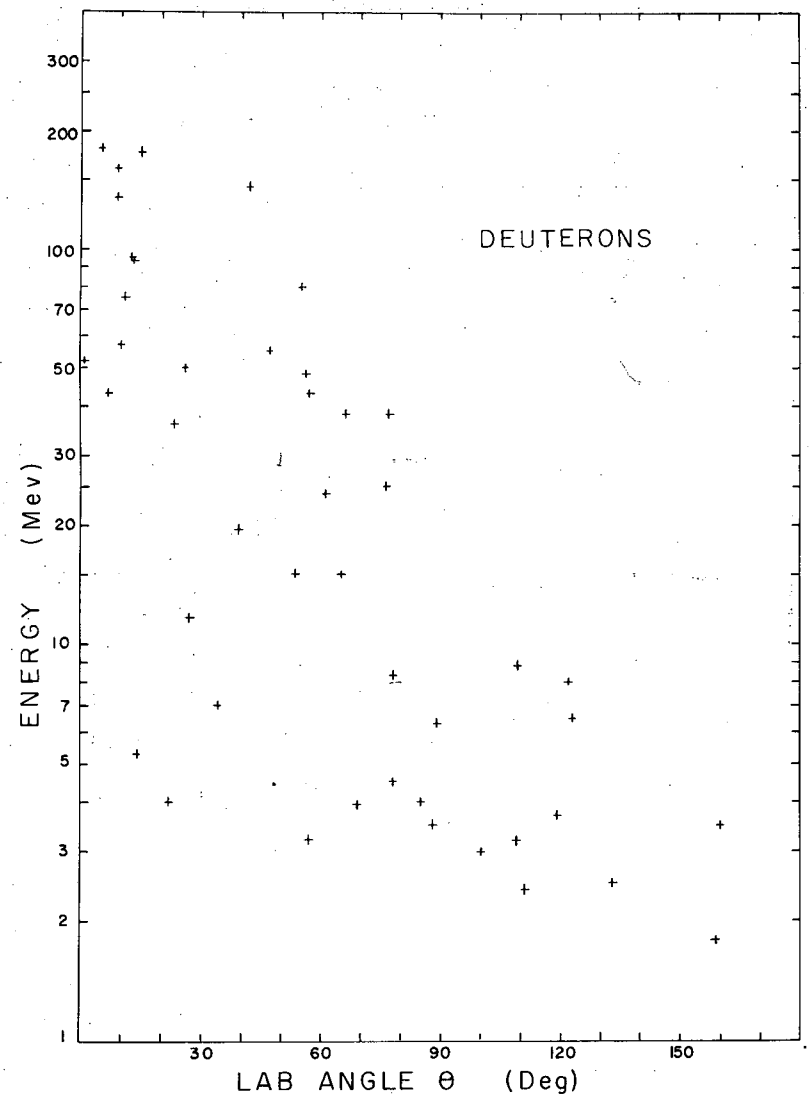

Deuterons from oxygen

Distribution in angle and energy of the single deuterons knocked out of oxygen (line 2 of Table I) by 300-Mev neutrons. The error figure of the previous diagram applies here also.

APPENDIX II

Representative Stars in Oyxgen Gas

The accompanying photograph shows oxygen stars typical of those analyzed. The neutron beam direction is from top to bottom, parallel to a line through the five alignment crosses. In addition to the stars, many tracks due to protons knocked out of the forward wall of the chamber are visible. The six-prong star (D) is a beautiful example of symmetric breakup. The two stars near the bottom of the photograph are typical examples of five-prong stars showing three α-particles, with two of these of approximately the same range. The following table shows the results of measurements on four of the stars, as lettered.

Star	Prong	Identi-fication	Radius of Curvature (cm)	Relative Ionization (approx.)	α (deg)	β (deg)	T (±10%) (Mev)
A	1	d	156	4	- 9	+ 0.5	260
	2	t	33	50	+50	- 9	8
	3	α	18	400	-11	-134	8
	4	α	13	600	+20	+125	6
	5	α	(range 0.4 cm)		~ 0	+136	1
B	1	p	31	12	-16	+ 88	22
	2	R(=N)	(0.45 cm)		+16	+135	-
C	1	p	35	10	- 5	- 10	29
	2	d	20	80	+14	+ 36	5.5
	3	R(=C)	(0.3 cm)		~+30	-140	-
D	1	d	31	40	+ 2	- 70	11
	2	p	29	15	- 7	-177	20
	3	d	23.5	60	0	+101	6
	4	α	(range 5.4 cm)		+35	+ 42	8
	5	α	(range 3.3 cm)		+35	+ 37	6
	6	p	(range 7.4 cm)		+36	+ 19	2.5

ρ is positive below the plane of the photograph

β is positive counterclockwise from the forward direction

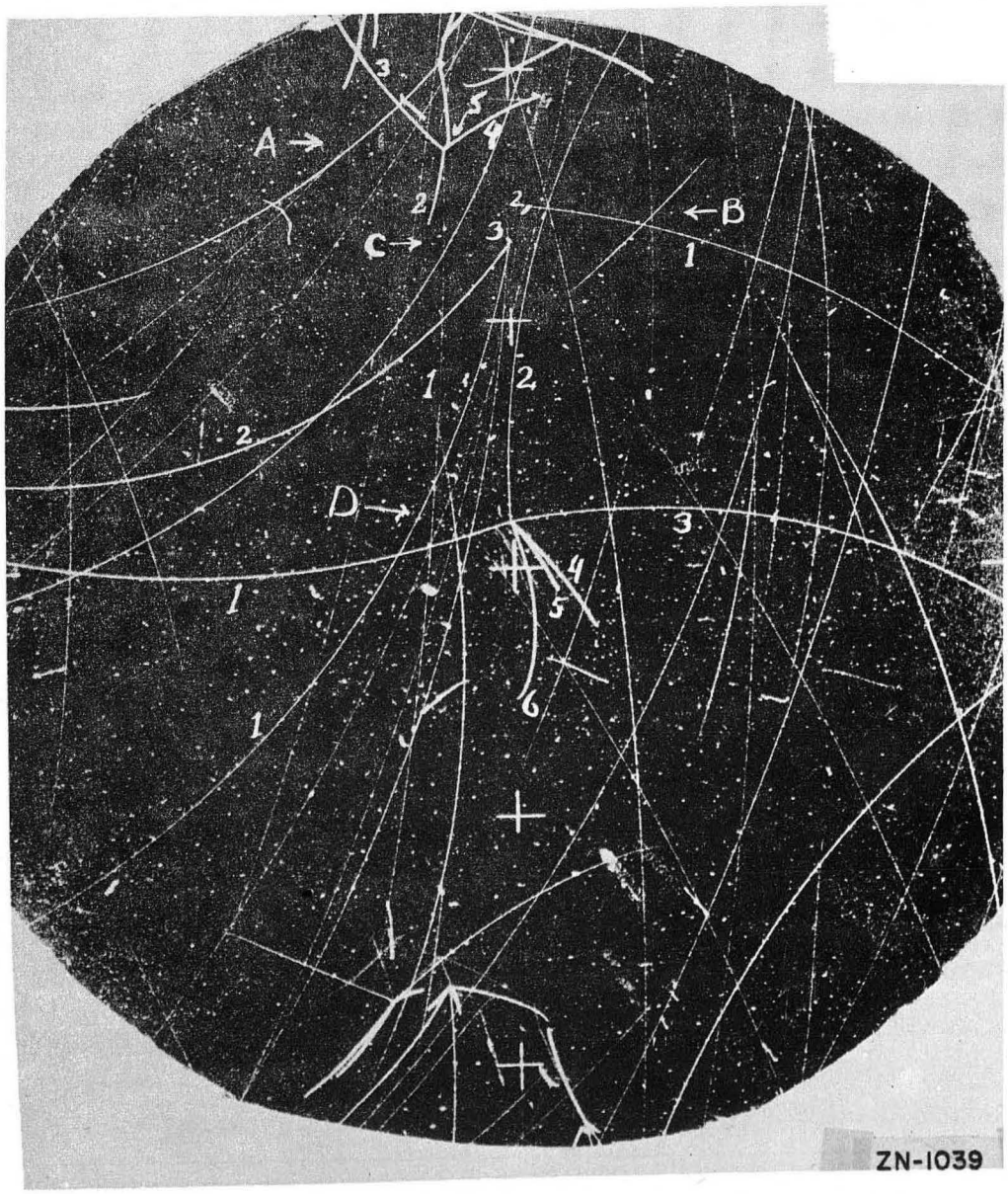
A
B
C
D
ZN-1039

APPENDIX III

Transformation from Angles α and β to Angles ϕ and θ

A. Derivation of Geometrical Formulae

Let $\vec{i}$, $\vec{j}$, and $\vec{k}$ be a set of orthogonal unit vectors, with $\vec{i}$ along the direction of the neutron beam, and let $\vec{r}_o$ be a unit vector along the tangent to the track at the origin of the star. The measured angles α and β and the laboratory angles ϕ and θ are then as shown in the figure below. We may write

$$\vec{r}_o = \vec{i} \cos \alpha \cos \beta + \vec{j} \cos \alpha \sin \beta + \vec{k} \sin \alpha$$

$$\text{and} \quad \vec{r}_o = \vec{i} \cos \theta \qquad + \vec{j} \sin \theta \cos \phi + \vec{k} \sin \theta \sin \phi.$$

By equating corresponding components, we obtain

$$\cos \theta = \cos \alpha \cos \beta, \tag{1}$$

$$\cos \alpha \sin \beta = \sin \theta \cos \phi, \tag{2}$$

$$\sin \alpha = \sin \theta \sin \phi. \tag{3}$$

Dividing (3) by (2) and rearranging,

$$\tan \alpha = \sin \beta \tan \phi. \tag{4}$$

Dividing (2) by (1) and rearranging,

$$\tan \beta = \cos \phi \tan \theta. \tag{5}$$

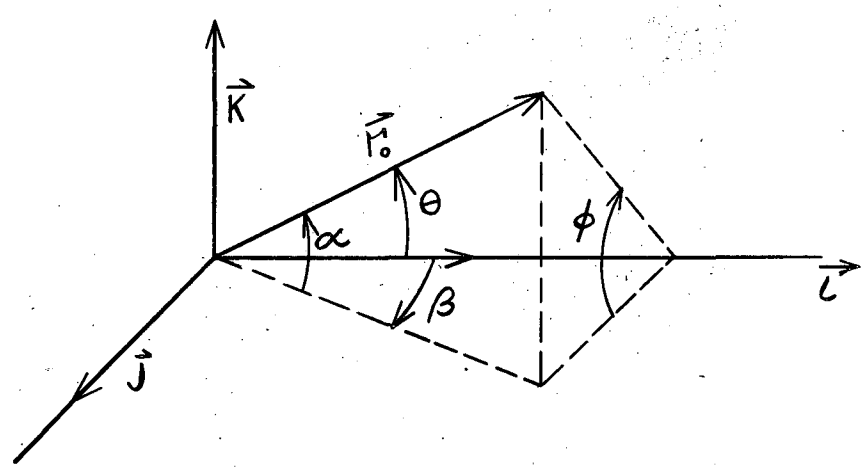

B. Nomograph Used in Transformation of Angles

The nomograph shown below, as furnished by John DePangher, was used first with Eq. (4) above to obtain angle ϕ, and then with Eq. (5) above (using $\sin\left[90 - \phi\right] = \cos\phi$) to obtain angle θ.

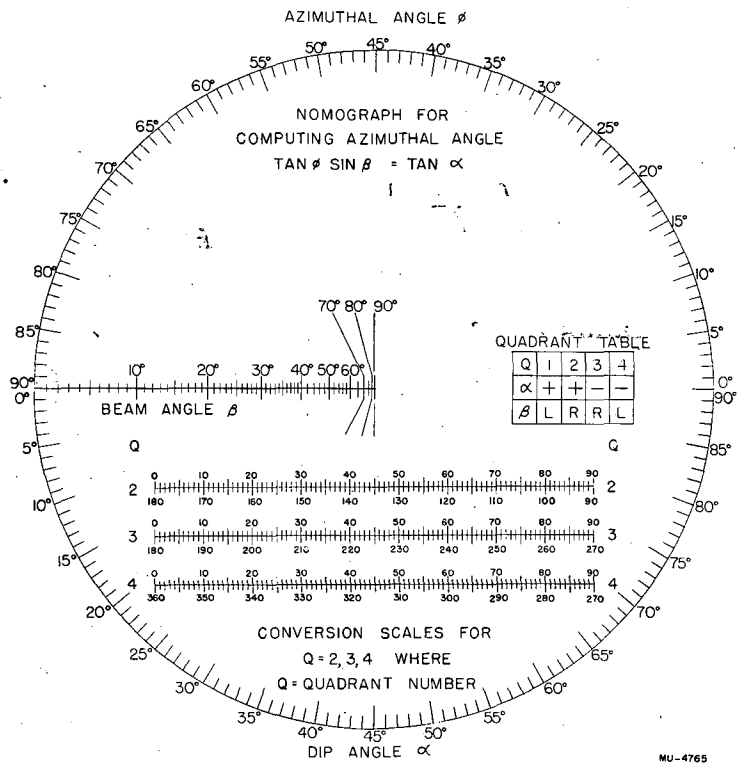

REFERENCES

1. V. Weisskopf, Phys. Rev. 52, 295 (1937).
2. K. J. Le Couteur, Proc. Phys. Soc. (London) A63, 259 (1950).
3. N. Bohr, Nature 137, 344 (1936).
4. R. Serber, Phys. Rev. 72, 1114 (1947).
5. M. Goldberger, Phys. Rev. 74, 1269 (1948).
6. J. Hadley and H. York, Phys. Rev. 80, 345 (1950).
7. K. Brueckner and W. Powell, Phys. Rev. 75, 1274 (1949).
8. G. Chew and M. Goldberger, Phys. Rev. 77, 470 (1950).
9. G. Bernardini, E. T. Booth, and S. J. Lindenbaum, Phys. Rev. 85, 826 (1952) and 88, 1017 (1952).
10. H. McManus, W. T. Sharpe, and H. Gellman, Phys. Rev. 93, 924 (1954).
11. H. McManus and W. T. Sharpe, private communication.
12. N. Feather, Proc. Roy. Soc. 141, 194 (1933).
13. William P. Ball, Nuclear Scattering of 300-Mev Neutrons, University of California Radiation Laboratory Report No. UCRL-1938, August 1952.
14. Marian Whitehead, private communication.
15. Roger H. Hildebrand, Donald A. Hicks, and Wesley H. Harker, Summary of Neutron Cross Section Measurements for 14-Mev to 280-Mev Neutrons, University of California Radiation Laboratory Report No. UCRL-1305, May 1951.
16. B. H. Bransden, Proc. Phys. Soc. A65, 738 (1952).
17. Wilmot N. Hess, The Production of Deuterons in High-Energy Nucleon Bombardment of Nuclei, and Its Bearing on Nuclear Charge Distribution, University of California Radiation Laboratory Report No. UCRL-2670, July 1954.
18. W. M. Powell, Rev. Sci. Instr. 20, 403 (1949).
19. K. Brueckner, W. Hartsough, E. Hayward, and W. Powell, Phys. Rev. 75, 555 (1949).
20. Donald Johnson, Energy and Ionization of Light Particles as a Function of Hρ, University of California Radiation Laboratory Report No. UCRL-1445, August 1951.

21. John DePangher, Jr., private communication.

22. Franklin C. Ford, The Production of Charged Pi Mesons by Neutrons on Oxygen, University of California Radiation Laboratory. Report No. UCRL-2148, March 1953.

Physics Dept.
Sacramento State College